





Extended Skyrme momentum-dependent potential in asymmetric nuclear matter and transport models

Junping Yang ¹, Xiang Chen ¹, Ying Cui,¹ Yangyang Liu ¹, Zhuxia Li,¹ and Yingxun Zhang ^{1,2,*}

¹China Institute of Atomic Energy, Beijing 102413, China

²Guangxi Key Laboratory of Nuclear Physics and Technology, Guangxi Normal University, Guilin 541004, China



(Received 6 November 2023; revised 4 February 2024; accepted 23 April 2024; published 30 May 2024)

Based on an extended Skyrme momentum-dependent interaction (MDI), we derive an isospin asymmetric equation of state, isospin-dependent single-particle potential and the Hamiltonian which can be used in the Boltzmann-Uehling-Uhlenbeck model and the quantum molecular dynamics (QMD) model at the beam energy less than 1 GeV/u. As an example of the applications of extended Skyrme MDI, we also present the results obtained with the extended Skyrme momentum-dependent interaction in the improved quantum molecular dynamics model (ImQMD), and the influence of the effective-mass splitting on the isospin sensitive observables, i.e., the single and double neutron-to-proton ratios, is discussed again.

DOI: [10.1103/PhysRevC.109.054624](https://doi.org/10.1103/PhysRevC.109.054624)

I. INTRODUCTION

The isospin asymmetric nuclear equation of state (EOS) plays a crucial role in understanding various properties of neutron stars, including the mass-radius relationship [1,2], tidal deformability [3], neutron-star mergers [3–5] and core-collapse of supernovae [6–8]. Numerous efforts have been made to constrain the isospin asymmetric nuclear EOS, particularly the symmetry energy at densities below $3\rho_0$ [9–16]. However, our understanding of the dependence of the neutron-star EOS on temperature and constituents such as neutrons, protons and baryons, is limited when relying solely on the properties of neutron stars.

The dependence of the symmetry energy on temperature and constituents can be extracted from heavy ion collisions (HICs) [17,18]. Up to now, some important progresses on the constraints of the density dependence of the symmetry energy via HICs have been obtained [12,15,19–23], but the discrepancy between the constraints from HICs and from the neutron stars was also observed [23,24]. One of the possibilities is the momentum-dependent symmetry potential. The different forms of the momentum-dependent symmetry potential can lead to the same density dependence of symmetry energy, which results in the same properties of neutron stars but different effects on the isospin sensitive observables [25–30].

The momentum-dependent symmetry potential is calculated from the difference between the single-particle potential of the neutron V_n and the proton V_p over the isospin asymmetry of the system δ , i.e., $V_{\text{sym}} = (V_n - V_p)/2\delta$ [31]. In general, the single-particle potential $V_{q=n,p}$ is composed of the momentum-independent potential and the momentum-dependent potential. Especially, the isospin-dependent momentum-dependent potential is not clearly known. Thus, constraining the isospin-dependent momentum-

dependent potential becomes one of the important topics in heavy ion collisions, and it heavily rely on the transport models. The strategy of constraining the form of neutron and proton single-particle potential with HICs need to assume the form of isospin-dependent MDI in advance, and then simulate the HICs with different isospin-dependent MDI in the transport model. By comparing the calculations to the data, one can constrain the isospin-dependent MDI indirectly.

The isospin-dependent momentum-dependent potential used in the transport models can be generally divided into three types. The first one is the square-type [26,27,32,33]

$$V_q(p) \propto \int d^3 p' f_q(\mathbf{r}, \mathbf{p}') (\mathbf{p} - \mathbf{p}')^2, \quad (1)$$

where $f_q(\mathbf{r}, \mathbf{p}')$ is the phase space distribution function [26,27,32,33] and had been used to study the effective mass splitting in HICs. This form is suitable for the HICs at the beam energy approximately less than 300 MeV/u [34] since it violates the optical potential extrapolated from the nucleon-nucleus reaction data. To fix this problem, the logarithm-type and Lorentzian-type momentum-dependent potential were proposed and used in the transport models. The isospin-dependent logarithm-type momentum-dependent single-particle potential is

$$V_q(p) \propto \int d^3 p' f_q(\mathbf{r}, \mathbf{p}') t_4 [\ln(t_5 (\mathbf{p} - \mathbf{p}')^2 + 1)]^2 \quad (2)$$

and was mainly used in QMD models [28,35–38]. The third one is the Lorentzian-type, and its single-particle potential is

$$V_q(p) \propto \int d^3 p' \frac{f_q(\mathbf{r}, \mathbf{p}')}{1 + (\mathbf{p} - \mathbf{p}')^2/\mu^2}. \quad (3)$$

Its isospin-dependent form was proposed in Ref. [39] and was widely used in QMD-type [40–43] and BUU-type models [39,44,45].

Theoretically, Eqs. (2) and (3) can only be calculated numerically in the framework of the QMD-type models, but it

*zhyx@ciae.ac.cn

will cost huge CPU time. To use the momentum-dependent interaction (MDI) conveniently, one approximate the results from Eqs. (2) and (3) by reformulating it with $|\mathbf{p}_i - \mathbf{p}_j|$ [46], where \mathbf{p}_i and \mathbf{p}_j are the average momentum of the i th and j th nucleons, respectively. The effect of the width of the wave packet was not explicitly involved. Therefore, modeling the isospin-dependent momentum-dependent potential with an appropriate shape over a wide beam energy region and explicitly considering the effect of the width of wave packet in the QMD type models is necessary. An extended Skyrme MDI [47,48] can meet this requirement since both the single-particle potential and the Hamiltonian with the Gaussian wave packet can be calculated analytically. Furthermore, it will also be useful in the BUU-type models and a pioneer work has been done in Ref. [48] for giving the nuclear equation of state and single-particle potential in nuclear matter.

This paper is organized as follows: In Sec. II, the form of the extended Skyrme MDI, the single-particle potential, the equation of state and the corresponding Hamiltonian used in the ImQMD model are given. In Sec. III, we present the numerical results on the equation of state, the symmetry energy and the single-particle potential in nuclear matter obtained with the extended Skyrme interactions. Then, we used the extended Skyrme MDI in the ImQMD and the effects of effective mass splitting on the neutron to proton yield ratios are simply rediscussed. Section IV is the summary and outlook.

II. FORMULAS

In the ImQMD model (-Sky version) [27], the Skyrme potential energy density without the spin-orbit term is used:

$$u_{\text{sky}} = u_{\text{loc}} + u_{\text{md}}. \quad (4)$$

The local potential energy density is

$$\begin{aligned} u_{\text{loc}} = & \frac{\alpha}{2} \frac{\rho^2}{\rho_0} + \frac{\beta}{\gamma + 1} \frac{\rho^{\gamma+1}}{\rho_0^\gamma} \\ & + \frac{g_{\text{sur}}}{2\rho_0} (\nabla \rho)^2 + \frac{g_{\text{sur,iso}}}{\rho_0} [\nabla(\rho_n - \rho_p)]^2 \\ & + A_{\text{sym}} \frac{\rho^2}{\rho_0} \delta^2 + B_{\text{sym}} \frac{\rho^{\gamma+1}}{\rho_0^\gamma} \delta^2. \end{aligned} \quad (5)$$

$\rho = \rho_n + \rho_p$ is the nucleon density and $\delta = (\rho_n - \rho_p)/\rho$ is the isospin asymmetry. The α is the parameter related to the two-body term, β and γ are related to the three-body term, g_{sur} and $g_{\text{sur,iso}}$ are related to the surface terms, A_{sym} and B_{sym} are the coefficients in the symmetry potential and come from the two- and three-body terms [36,49]. The nonlocal potential energy density is

$$\begin{aligned} u_{\text{md}} = & C_0 \sum_{ij} \int d^3 p d^3 p' f_i(\mathbf{r}, \mathbf{p}) f_j(\mathbf{r}, \mathbf{p}') (\mathbf{p} - \mathbf{p}')^2 \\ & + D_0 \sum_{ij \in n} \int d^3 p d^3 p' f_i(\mathbf{r}, \mathbf{p}) f_j(\mathbf{r}, \mathbf{p}') (\mathbf{p} - \mathbf{p}')^2 \\ & + D_0 \sum_{ij \in p} \int d^3 p d^3 p' f_i(\mathbf{r}, \mathbf{p}) f_j(\mathbf{r}, \mathbf{p}') (\mathbf{p} - \mathbf{p}')^2. \end{aligned} \quad (6)$$

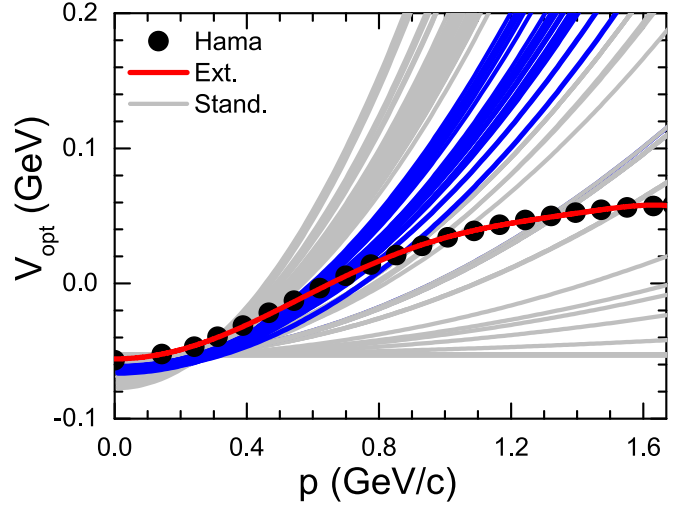


FIG. 1. Single-particle potentials obtained from the standard Skyrme MDI (gray lines and blue lines) and the extended Skyrme MDI (red line). The points are the data of single-particle potential obtained from Hama's data [51].

Here, $f_i(\mathbf{r}, \mathbf{p})$ is the phase space density distribution of particle i , i.e.,

$$f_i(\mathbf{r}, \mathbf{p}) = \frac{1}{(\pi \hbar)^3} e^{-\frac{(\mathbf{r}-\mathbf{r}_i)^2}{2\sigma_r^2} - \frac{(\mathbf{p}-\mathbf{p}_i)^2}{2\sigma_p^2}}.$$

The parameters in Eqs. (5) and (6) can be calculated directly from the standard Skyrme interaction [15,49], and we name it the standard Skyrme interaction or the standard Skyrme-type MDI in the following discussions.

The treatments of the collision term and isospin-dependent Pauli blocking effects are the same as those in Refs. [36,50]. The isospin-dependent in-medium nucleon-nucleon scattering cross sections in the collision term are assumed to be of the form $\sigma_{nn,pp/np}^* = (1 - \eta\rho/\rho_0)\sigma_{nn,pp/np}^{\text{free}}$, with η being a parameter that depends on the beam energy. The influence of extended MDI on the η is not discussed in this work.

In Fig. 1, we present the single-particle potentials in the nuclear matter obtained with the standard Skyrme interactions. The 123 Skyrme parameter sets (gray lines) are selected according to the current knowledge on the nuclear matter parameters [15], i.e., $K_0 = [200, 280]$ MeV, $S_0 = [25, 35]$ MeV, $L = [30, 120]$ MeV, $m_s^*/m = [0.6, 1.0]$, $f_1 = m/m_s^* - m/m_v^* = [-0.5, 0.4]$. At a momentum less than 0.8 GeV/c (the kinetic energy is less than 300 MeV), there are 25 Skyrme parameter sets (blue lines): BSk14, BSk15, BSk16, BSk17, BSk9, Gs, MSL0, Rs, Sefm081, SGII, SkM, SKMs, SV-mas08, SkRA, QMC650, QMC700, QMC750, KDE, KDE0v1, SkT7, SkT7a, SkT8, SkT8a, SkT9, and SkT9a can describe the Hama data with a reduced χ^2 is less than 0.7. Most have $m_n^* > m_p^*$ except for BSk9, KDE, KDE0v1. These single-particle potentials go infinity as the relative momentum increases, which violates the experimental data of the optical potential (solid points) [51]. This condition limits the utility of the standard Skyrme potential energy density in HICs at a beam energy below 300 MeV/u. Furthermore, the research of the scientific collaboration UNEDF-SciDAC [52,53] has

shown that there is no more room to improve the standard Skyrme functional to describe the nuclear and neutron stars by simply acting on the optimization procedure.

To overcome the above deficiency of the standard Skyrme interaction, an extended Skyrme effective interaction that includes the terms in relative momenta up to sixth order was proposed in Ref. [47]. The extended Skyrme interaction was stimulated by the idea that it is possible to expand a finite-range interaction in terms of a zero range like and such an expansion converges [54], and the central term can be written order by order as

$$\begin{aligned}
v_C = & t_0^{(0)}(1 + x_0^{(0)}P_\sigma)\delta(\mathbf{r}) \\
& + \frac{1}{2}t_1^{(2)}(1 + x_1^{(2)}P_\sigma)\delta(\mathbf{r})[\mathbf{k}^2 + \mathbf{k}'^2] \\
& + t_2^{(2)}(1 + x_2^{(2)}P_\sigma)\delta(\mathbf{r})\mathbf{k}' \cdot \mathbf{k} \\
& + \frac{1}{4}t_1^{(4)}(1 + x_1^{(4)}P_\sigma)\delta(\mathbf{r})[(\mathbf{k}^2 + \mathbf{k}'^2)^2 + 4(\mathbf{k}' \cdot \mathbf{k})^2] \\
& + t_2^{(4)}(1 + x_2^{(4)}P_\sigma)\delta(\mathbf{r})(\mathbf{k}' \cdot \mathbf{k})(\mathbf{k}^2 + \mathbf{k}'^2) \\
& + \frac{t_1^{(6)}}{2}(1 + x_1^{(6)}P_\sigma)\delta(\mathbf{r})(\mathbf{k}^2 + \mathbf{k}'^2)[(\mathbf{k}^2 + \mathbf{k}'^2)^2 \\
& + 12(\mathbf{k}' \cdot \mathbf{k})^2] \\
& + t_2^{(6)}(1 + x_2^{(6)}P_\sigma)\delta(\mathbf{r})(\mathbf{k}' \cdot \mathbf{k})[3(\mathbf{k}^2 + \mathbf{k}'^2)^2 + 4(\mathbf{k}' \cdot \mathbf{k})^2].
\end{aligned} \tag{7}$$

The first term in Eq. (7) is the local two-body interaction; the remaining terms are the nonlocal interaction with the power of the relative momentum up to six, i.e., \mathbf{k}^6 . P_σ is the spin-exchange operator and \mathbf{k} in Eq. (7) denotes the operator $(\nabla_1 - \nabla_2)/2i$ acting on the right, whereas, \mathbf{k}' is the operator $-(\nabla_1 - \nabla_2)/2i$ acting on the left. They are related to the relative momentum between two nucleons.

Inspired by this idea, we assume a phenomenological momentum-dependent interaction such as

$$g(\mathbf{p} - \mathbf{p}') = \sum_{l=0}^N b_l (\mathbf{p} - \mathbf{p}')^{2l} \tag{8}$$

in the transport models. The parameter b_l is used to determine the shape of the MDI, and its dimension is GeV^{2-2l} for keeping the dimension of $g(\mathbf{p} - \mathbf{p}')$ in GeV^2 . Consequently, the energy density u_{md} in Eq. (6) is replaced by

$$\begin{aligned}
u_{md} = & \tilde{C}_0 \sum_{ij} \int d^3p d^3p' f_i(\mathbf{r}, \mathbf{p}) f_j(\mathbf{r}, \mathbf{p}') g(\mathbf{p} - \mathbf{p}') \\
& + \tilde{D}_0 \sum_{ij \in n} \int d^3p d^3p' f_i(\mathbf{r}, \mathbf{p}) f_j(\mathbf{r}, \mathbf{p}') g(\mathbf{p} - \mathbf{p}') \tag{9} \\
& + \tilde{D}_0 \sum_{ij \in p} \int d^3p d^3p' f_i(\mathbf{r}, \mathbf{p}) f_j(\mathbf{r}, \mathbf{p}') g(\mathbf{p} - \mathbf{p}').
\end{aligned}$$

The number of N , the interaction parameters b_l , \tilde{C}_0 , and \tilde{D}_0 in Eqs. (8) and (9) can be determined by fitting the optical potential data or calculations from microscopic model, such as Dirac-Brueckner-Hartree-Fock [55].

At the given shape of MDI, i.e., given N and b_l , one can vary the form of symmetry potential, isoscalar effective mass, and the isovector effective mass through \tilde{C}_0 and \tilde{D}_0 , which have a dimension in fm^3/MeV . Their values are used to adjust the strength and form of the momentum-dependent symmetry potential for studying the uncertainty of the single-particle potential of neutron and proton in isospin asymmetric nuclear matter.

In the following part, we present the formulas for the single-particle potential and the equation of state, the nuclear matter parameters and their relations to the interaction parameters in transport models and the Hamiltonian used in the QMD-type models as well.

A. Single-particle potential and equation of state

The single-particle potential V_q in isospin asymmetric nuclear matter can be calculated by taking the functional derivative of the energy density with respect to the single-body phase space distribution of protons or neutrons $f_q(r, p)$,

$$\begin{aligned}
V_q(\rho, \delta, p) = & \frac{\delta u_{loc}}{\delta f_q} + \frac{\delta u_{md}}{\delta f_q} \\
= & V_q^{loc}(\rho, \delta) + V_q^{md}(\rho, \delta, p),
\end{aligned} \tag{10}$$

where $q = n$ or p . V_q^{loc} is

$$\begin{aligned}
V_q^{loc}(\rho, \delta) = & \frac{\delta u_{loc}}{\delta f_q} = \alpha \frac{\rho}{\rho_0} + \beta \frac{\rho^\gamma}{\rho_0^\gamma} + (\gamma - 1) B_{\text{sym}} \frac{\rho^\gamma}{\rho_0^\gamma} \delta^2 \\
& \pm 2 \left[A_{\text{sym}} \frac{\rho}{\rho_0} + B_{\text{sym}} \left(\frac{\rho}{\rho_0} \right)^\gamma \right] \delta.
\end{aligned} \tag{11}$$

The sign “+” is for neutrons, and “−” is for protons.

V_q^{md} is

$$\begin{aligned}
V_q^{md}(\rho, \delta, p) = & \frac{\delta u_{md}}{\delta f_q} = 2\tilde{C}_0 \int d^3p' f(\mathbf{r}, \mathbf{p}') g(\mathbf{p} - \mathbf{p}') \\
& + 2\tilde{D}_0 \int d^3p' f_q(\mathbf{r}, \mathbf{p}') g(\mathbf{p} - \mathbf{p}').
\end{aligned} \tag{12}$$

The form of Eqs. (11) and (12) can be directly used in transport models for simulating heavy ion collisions by using the phase space density $f_q(\mathbf{r}, \mathbf{p})$ obtained in solving the transport equation. Then, the environment of the nucleons changes, such as the density, isospin asymmetry, and temperature of the environment, from the initial to the final stage in the heavy-ion collision will be automatically involved.

To quantitatively understand the properties of the extended Skyrme MDI, the single-particle potential and equation of state in the cold nuclear matter are analyzed and compared with that obtained with standard Skyrme interaction. In cold nuclear matter,

$$\begin{aligned}
f_q(\mathbf{r}, \mathbf{p}') = & \left(\frac{4\pi}{3} p_{F_q}^3 \right)^{-1} \rho_q \Theta(p_{F_q} - |p'|) \\
= & \frac{2}{(2\pi\hbar)^3} \Theta(p_{F_q} - |p'|),
\end{aligned} \tag{13}$$

and $p_{F_q} = \hbar(3\pi^2\rho_q)^{1/3}$. Thus, the corresponding V_q^{md} can also be written in an analytical form:

$$V_q^{md}(\rho, \delta, p) = 2\tilde{C}_0 \left[\sum_{l=1}^N b_l \sum_{l=0, l \in \text{even}}^{2l} \tilde{A}_{ll} \sum_{q=n, p} \rho_q^{(2l-l+3)/3} p^l \right] + 2\tilde{D}_0 \left[\sum_{l=1}^N b_l \sum_{l=0, l \in \text{even}}^{2l} \tilde{A}_{ll} \rho_q^{(2l-l+3)/3} p^l \right], \quad (14)$$

and

$$\tilde{A}_{ll} = \frac{2}{(2\pi\hbar)^3} 4\pi \left\{ [\hbar(3\pi^2)^{1/3}]^{(2l-l+3)} \binom{2l}{l} \frac{1}{(2l-l+3)} \right\}.$$

Here, $\binom{2l}{l}$ represents the number of combinations of l elements selected from $2l$ elements. One should note that the summation of b_l in Eq. (14) starts from b_1 . The value of b_0 will be related to the strength of the local potential when we use the extended Skyrme energy density functional.

Furthermore, the single-particle potential V_q as in Eq. (10) can be expanded as a power series of isospin asymmetry δ , by using the $\rho_q = \frac{\rho}{2}(1 + \tau_q\delta)$, with $\tau_q = 1$ or -1 for neutrons and protons. The so-called Lane potential [31] means one neglects the higher-order terms ($\delta^2, \delta^3, \dots$), i.e.,

$$V_q = V_0 \pm V_{\text{sym}}\delta + \dots \quad (15)$$

V_0 is

$$V_0 = \alpha \frac{\rho}{\rho_0} + \beta \frac{\rho^\gamma}{\rho_0^\gamma} + 4 \left(\tilde{C}_0 + \frac{\tilde{D}_0}{2} \right) \times \left[\sum_{l=1}^N b_l \sum_{l=0, l \in \text{even}}^{2l} \tilde{A}_{ll} \left(\frac{\rho}{2} \right)^{(2l-l+3)/3} p^l \right]. \quad (16)$$

V_{sym} is,

$$V_{\text{sym}} = 2A_{\text{sym}} \frac{\rho}{\rho_0} + 2B_{\text{sym}} \left(\frac{\rho}{\rho_0} \right)^\gamma + 2\tilde{D}_0 \left[\sum_{l=1}^N b_l \sum_{l=0, l \in \text{even}}^{2l} \tilde{A}_{ll} \frac{2l-l+3}{3} \times \left(\frac{\rho}{2} \right)^{(2l-l+3)/3} p^l \right]. \quad (17)$$

The first and second terms in Eq. (17) are the momentum-independent parts of the symmetry potential, and the last term is the momentum-dependent part of the symmetry potential.

The isospin asymmetric equation of state for cold nuclear matter reads

$$E/A(\rho, \delta) = \frac{3\hbar^2}{10m} \left(\frac{3\pi^2}{2} \rho \right)^{2/3} + \frac{\alpha}{2} \frac{\rho}{\rho_0} + \frac{\beta}{\gamma+1} \frac{\rho^\gamma}{\rho_0^\gamma} + \left(\tilde{C}_0 + \frac{\tilde{D}_0}{2} \right) \sum_{l=1}^N \tilde{g}_{md}^{(l)} \rho^{2l/3+1} + S(\rho)\delta^2 + \dots \quad (18)$$

The coefficient of $\tilde{g}_{md}^{(l)}$ is

$$\tilde{g}_{md}^{(l)} = \frac{4b_l}{2^{(2l+6)/3}} \sum_{l=0, l \in \text{even}}^{2l} \mathcal{G}_{ll}, \quad (19)$$

with \mathcal{G}_{ll} being

$$\mathcal{G}_{ll} = \left(\frac{2}{(2\pi\hbar)^3} \right)^2 (4\pi)^2 \left\{ [\hbar(3\pi^2)^{1/3}]^{(2l+6)} \binom{2l}{l} \times \frac{1}{(l+3)} \frac{1}{(2l-l+3)} \right\},$$

which has a constant value at a given l , and l and is independent of b_l .

The density dependence of the symmetry energy $S(\rho)$ becomes

$$S(\rho) = \frac{\hbar^2}{6m} \left(\frac{3\pi^2\rho}{2} \right)^{2/3} + A_{\text{sym}} \frac{\rho}{\rho_0} + B_{\text{sym}} \left(\frac{\rho}{\rho_0} \right)^\gamma + \sum_{l=1}^N \tilde{C}_{\text{sym}}^{(l)} \rho^{2l/3+1}. \quad (20)$$

Here $\tilde{C}_{\text{sym}}^{(l)}$ is

$$\tilde{C}_{\text{sym}}^{(l)} = 2\tilde{C}_0 \left[\frac{b_l}{2^{(2l+6)/3}} \sum_{l=0, l \in \text{even}}^{2l} \mathcal{G}_{ll} \times \left(\frac{l+3}{3} \frac{l}{3} + \frac{2l-l+3}{3} \frac{2l-l}{3} \right) \right] + \tilde{D}_0 \left[\frac{b_l}{2^{(2l+6)/3}} \frac{2l+6}{3} \frac{2l+3}{3} \sum_{l=0, l \in \text{even}}^{2l} \mathcal{G}_{ll} \right]. \quad (21)$$

which is the l th coefficient of the extended Skyrme-type MDI term in the symmetry energy. The derivations of the energy density and the single-particle potential can be found in Appendixes A and B.

The single-particle potential, EOS, and symmetry energy at finite temperature can be obtained by using Eqs. (11), (12), and (9) by replacing f with the Fermi distribution at a certain temperature and solving these equations with the same method as in Ref. [56]. Our calculations show that the difference of single-particle potential between $T = 0$ and $T = 20$ MeV is less than 9% at the momentum less than 500 MeV/ c , and similar at momenta greater than 500 MeV/ c .

B. Nuclear matter parameters and its relation to the interaction parameters

To investigate the uncertainty of the neutron and proton single-particle potential in isospin asymmetric nuclear matter, one may vary it by adjusting the effective nuclear interaction parameters in the transport models. However, directly adjusting the effective nuclear interaction parameters always mixes the contributions from the isoscalar and isovector part of single-particle potential. To isolate the contributions from the isoscalar and isovector part of the effective interaction, one can set the nuclear matter parameters as an input variable in

the transport models. The advantages of using nuclear matter parameters as input are as similar as in Refs. [15,57,58]. First, the nuclear matter parameters have a precise physical meaning. Second, the Bayesian analysis in transport model simulations in the nuclear matter parameter space can be easily performed, and the uncertainty of the theoretical predictions for all bulk properties can be directly obtained.

In this work, the parameters used in the extended Skyrme interaction as in Eq. (18), i.e., α , β , γ , A_{sym} , B_{sym} , \tilde{C}_0 , and \tilde{D}_0 , can be obtained from the nuclear matter parameters by the same standard protocol as in the standard Skyrme interaction [15]. They are realized by solving the seven equations for the determination of the saturation density ρ_0 , the energy per nucleon at saturation density E_0 , the incompressibility K_0 , the isoscalar effective mass m_s^* , the isovector effective mass m_v^* , the symmetry energy coefficient $S(\rho_0)$ and the slope of the symmetry energy L .

The first equation is related to the value of the saturation density ρ_0 which is obtained by seeking the root of the following equation:

$$P = \rho_0^2 \frac{d}{d\rho} \frac{E}{A}(\rho_0, \delta = 0) = 0, \quad (22)$$

i.e.,

$$\begin{aligned} & \frac{2}{5}\epsilon_F^0 \rho_0 + \frac{\alpha}{2}\rho_0 + \frac{\beta}{\gamma+1}\gamma\rho_0 \\ & + \left(\tilde{C}_0 + \frac{\tilde{D}_0}{2}\right) \sum_{l=1}^N \tilde{g}_{md}^{(l)} \left(\frac{2l}{3} + 1\right) \rho_0^{2l/3+2} = 0, \end{aligned} \quad (23)$$

where

$$\epsilon_F^0 = \frac{\hbar^2}{2m} \left(\frac{3\pi^2 \rho_0}{2}\right)^{2/3}.$$

The second equation is the binding energy E_0 . It reads

$$\begin{aligned} E_0 &= E/A(\rho_0) \\ &= \frac{3}{5}\epsilon_F^0 + \frac{\alpha}{2} + \frac{\beta}{\gamma+1} + \left(\tilde{C}_0 + \frac{\tilde{D}_0}{2}\right) \sum_{l=1}^N \tilde{g}_{md}^{(l)} \rho_0^{2l/3+1}. \end{aligned} \quad (24)$$

The third equation is the incompressibility K_0 , i.e.,

$$\begin{aligned} K_0 &= 9\rho_0^2 \left. \frac{\partial^2 E/A}{\partial \rho^2} \right|_{\rho_0} \\ &= \frac{-6}{5}\epsilon_F^0 + 9\frac{\beta}{\gamma+1}\gamma(\gamma-1) \\ &+ 6\left(\tilde{C}_0 + \frac{\tilde{D}_0}{2}\right) \sum_{l=1}^N \tilde{g}_{md}^{(l)} \left(\frac{2l}{3} + 1\right) l \rho_0^{2l/3+1}. \end{aligned} \quad (25)$$

The fourth and fifth equations are related to the neutron and proton effective mass or the isoscalar and isovector effective mass. The neutron and proton effective mass are obtained from the neutron and proton potential according to

$$\frac{m}{m_q^*} = 1 + \frac{m}{p} \frac{\partial V_q}{\partial p}, \quad q = n, p. \quad (26)$$

The neutron and proton effective mass will be

$$\begin{aligned} \frac{m}{m_q^*} &= 1 + 2\tilde{C}_0 m \left[\sum_{l=1}^N b_l \sum_{l=0, l \in \text{even}}^{2l} \tilde{A}_{ll} \sum_q \rho_q^{(2l-l+3)/3} l p^{l-2} \right] \\ &+ 2\tilde{D}_0 m \left[\sum_{l=1}^N b_l \sum_{l=0, l \in \text{even}}^{2l} \tilde{A}_{ll} \rho_q^{(2l-l+3)/3} l p^{l-2} \right]. \end{aligned} \quad (27)$$

Then, we can find the relationship between $\Delta m_{np}^* = (m_n^* - m_p^*)/m$ and V_{sym} as

$$\Delta m_{np}^* \approx -\left(\frac{m^*}{m}\right)^2 4m\delta \frac{\partial V_{\text{sym}}}{\partial p^2}, \quad (28)$$

The derivation can be found in Appendix C. It means that the strength of the effective mass splitting Δm_{np}^* depends on the momentum-dependent part of the symmetry potential when the m^*/m is fixed.

The isoscalar effective mass m_s^* can be obtained at $\rho_q = \rho/2$ from Eq. (27), and the isovector effective mass m_v^* can be obtained at $\rho_q = 0$ which represents the neutron (proton) effective mass in pure proton (neutron) matter as in Refs. [59,60]. They are

$$\begin{aligned} \frac{m}{m_s^*}(\rho, p) &= 1 + 4\left(\tilde{C}_0 + \frac{\tilde{D}_0}{2}\right) m \\ &\times \left[\sum_{l=1}^N b_l \sum_{l=0, l \in \text{even}}^{2l} \tilde{A}_{ll} \left(\frac{\rho}{2}\right)^{(2l-l+3)/3} l p^{l-2} \right], \\ \frac{m}{m_v^*}(\rho, p) &= 1 + 4\tilde{C}_0 m \\ &\times \left[\sum_{l=1}^N b_l \sum_{l=0, l \in \text{even}}^{2l} \tilde{A}_{ll} \left(\frac{\rho}{2}\right)^{(2l-l+3)/3} l p^{l-2} \right]. \end{aligned} \quad (29)$$

As same as in Ref. [27], we define a quantity f_l ,

$$\begin{aligned} f_l(\rho, p) &= \frac{m}{m_s^*} - \frac{m}{m_v^*} \\ &= 2\tilde{D}_0 m \left[\sum_{l=1}^N b_l \sum_{l=0, l \in \text{even}}^{2l} \tilde{A}_{ll} \left(\frac{\rho}{2}\right)^{(2l-l+3)/3} l p^{l-2} \right], \end{aligned} \quad (30)$$

to describe the isospin effective mass splitting, which has the opposite sign with Δm_{np}^* . In practical transport model calculations, Δm_{np}^* depends on the power expansion of isospin asymmetry and cannot be used to calculate the \tilde{D}_0 accurately. Thus, in the determination of interaction parameters in the transport models, we use the values of m_s^*/m and f_l .

The sixth and seventh equations are the symmetry energy coefficient S_0 ,

$$S_0 = S(\rho_0) = \frac{1}{3}\epsilon_F^0 + A_{\text{sym}} + B_{\text{sym}} + \sum_{l=1}^N \tilde{C}_{\text{sym}}^{(l)} \rho_0^{2l/3+1}, \quad (31)$$

and the slope of the symmetry energy L is

$$L = 3\rho_0 \left. \frac{\partial S(\rho)}{\partial \rho} \right|_{\rho_0} = \frac{2}{3}\epsilon_F^0 + 3A_{\text{sym}} + 3B_{\text{sym}}\gamma + 3 \sum_{l=1}^N \tilde{C}_{\text{sym}}^{(l)} \left(\frac{2l}{3} + 1 \right) \rho_0^{2l/3+1}. \quad (32)$$

Given the values S_0, L, K_0, E_0 , and $\rho_0, f_I^0 = f_I(\rho_0, p_F)$ and $m/m_{s0}^* = \frac{m}{m_{s0}^*}(\rho_0, p_F)$, the coefficients $\alpha, \beta, \gamma, A_{\text{sym}}, B_{\text{sym}}, \tilde{C}_0$, and \tilde{D}_0 can be obtained according to the following formulas:

$$\tilde{D}_0 = f_I^0 / \left[2m \sum_{l=1}^N b_l \sum_{l=0, l \in \text{even}}^{2l} \tilde{A}_{ll} \left(\frac{\rho_0}{2} \right)^{(2l-l+3)/3} l p_F^{l-2} \right]. \quad (33)$$

$$\tilde{C}_0 = \left(\frac{m}{m_{s0}^*} - 1 \right) / \left[4m \sum_{l=1}^N b_l \times \sum_{l=0, l \in \text{even}}^{2l} \tilde{A}_{ll} \left(\frac{\rho_0}{2} \right)^{(2l-l+3)/3} l p_F^{l-2} \right] - \frac{\tilde{D}_0}{2}. \quad (34)$$

$$\gamma = \frac{K_0 + \frac{6}{5}\epsilon_F^0 - 6(\tilde{C}_0 + \frac{\tilde{D}_0}{2}) \sum_{l=1}^N \left(\frac{2l}{3} + 1 \right) I \rho_0^{\frac{2l}{3}+1} \tilde{g}_{md}^{(l)}}{\frac{9}{5}\epsilon_F^0 - 6(\tilde{C}_0 + \frac{\tilde{D}_0}{2}) \sum_{l=0}^N I \rho_0^{\frac{2l}{3}+1} \tilde{g}_{md}^{(l)} - 9E_0},$$

$$\beta = \frac{[\frac{1}{5}\epsilon_F^0 - \frac{2}{3}(\tilde{C}_0 + \frac{\tilde{D}_0}{2}) \sum_{l=1}^N I \rho_0^{\frac{2l}{3}+1} \tilde{g}_{md}^{(l)} - E_0](\gamma + 1)}{\gamma - 1},$$

$$\alpha = 2E_0 - 2 \left(\tilde{C}_0 + \frac{\tilde{D}_0}{2} \right) \sum_{l=1}^N \rho_0^{\frac{2l}{3}+1} \tilde{g}_{md}^{(l)} - \frac{6}{5}\epsilon_F^0 - \frac{2\beta}{\gamma + 1},$$

$$B_{\text{sym}} = \frac{3S_0 - L - \frac{1}{3}\epsilon_F^0 + 2 \sum_{l=1}^N I \tilde{C}_{\text{sym}}^{(l)} \rho_0^{\frac{2l}{3}+1}}{-3(\gamma - 1)},$$

$$A_{\text{sym}} = S_0 - \frac{1}{3}\epsilon_F^0 - B_{\text{sym}} - \sum_{l=1}^N \tilde{C}_{\text{sym}}^{(l)} \rho_0^{\frac{2l}{3}+1}. \quad (35)$$

C. Hamiltonian from extended Skyrme momentum-dependent interaction in the quantum molecular dynamics type models

Here, we give an example of the Hamiltonian of the extended Skyrme MDI in the QMD-type models. The energy density of the extended Skyrme MDI can be obtained by folding the interaction with the wave function or with the phase space density as in Eq. (9).

In the framework of the ImQMD model, the result of the integration term $I_{ij} = \int d^3 p d^3 p' f_i(\mathbf{r}, \mathbf{p}) f_j(\mathbf{r}, \mathbf{p}') g(\mathbf{p} - \mathbf{p}')$

Eq. (9) is

$$\begin{aligned} I_{ij} &= \int d^3 p d^3 p' f_i(\mathbf{r}, \mathbf{p}) f_j(\mathbf{r}, \mathbf{p}') g(\mathbf{p} - \mathbf{p}') \\ &= \frac{1}{(2\pi\sigma_r^2)^3} \frac{1}{(\pi\sigma_p^2)^{1/2}} \exp \left[-\frac{(\mathbf{r} - \mathbf{r}_i)^2}{2\sigma_r^2} - \frac{(\mathbf{r} - \mathbf{r}_j)^2}{2\sigma_r^2} \right] \\ &\quad \times \sum_{l=1}^N b_l \sum_{l=0, l \in \text{even}}^{2l+1} \binom{2l+1}{l} (\mathbf{p}_i - \mathbf{p}_j)^{2l-l} W(l, \sigma_p). \end{aligned} \quad (36)$$

Here, $W(l, \sigma_p)$ are the contributions from the width of the wave packet and they are

$$\begin{aligned} W(0, \alpha = 1/4\sigma_p^2) &= \frac{\sqrt{\pi}}{2\alpha^{1/2}} = \sqrt{\pi}\sigma_p, \\ W(1, \alpha = 1/4\sigma_p^2) &= \frac{1}{2\alpha} = 2\sigma_p^2, \\ &\vdots \\ W(l, \alpha = 1/4\sigma_p^2) &= -\frac{\partial}{\partial \alpha} W(l-2, \sigma_p). \end{aligned} \quad (37)$$

The integration of I_{ij} over the coordinate space is

$$\begin{aligned} \int I_{ij} d^3 r &= \rho_{ij} \sum_{l=1}^N b_l \sum_{l=0, l \in \text{even}}^{2l+1} \binom{2l+1}{l} (\mathbf{p}_i - \mathbf{p}_j)^{2l-l} \\ &\quad \times \frac{W(l, \sigma_p)}{(\pi\sigma_p^2)^{1/2}}, \end{aligned} \quad (38)$$

and thus the corresponding part of Hamiltonian is

$$\begin{aligned} H &= 2\tilde{C}_0 \sum_{ij} \rho_{ij} \sum_{l=1}^N b_l \sum_{l=0, l \in \text{even}}^{2l+1} \binom{2l+1}{l} (\mathbf{p}_i - \mathbf{p}_j)^{2l-l} \\ &\quad \times \frac{W(l, \sigma_p)}{(\pi\sigma_p^2)^{1/2}} + (\tilde{C}_0 + \tilde{D}_0) \sum_{ij \in q} \rho_{ij} \sum_{l=1}^N b_l \\ &\quad \times \sum_{l=0, l \in \text{even}}^{2l+1} \binom{2l+1}{l} (\mathbf{p}_i - \mathbf{p}_j)^{2l-l} \frac{W(l, \sigma_p)}{(\pi\sigma_p^2)^{1/2}}, \end{aligned} \quad (39)$$

where

$$\rho_{ij} = \frac{1}{(4\pi\sigma_r^2)^{3/2}} \exp \left[-\frac{(\mathbf{r}_i - \mathbf{r}_j)^2}{4\sigma_r^2} \right]. \quad (40)$$

III. RESULTS AND DISCUSSIONS

A. Determination of the expansion number N and coefficient b_l

The values of N, b_l, \tilde{C}_0 , and \tilde{D}_0 are obtained by fitting the $V_0(\rho_0, p)$ in Eq. (16) to Hama's optical potential data [51], which gives the isoscalar effective mass $m_{s0}^*/m = 0.77$. One should note that the data can be well described when $N \geq 4$. As an example, we present the fitting results with extended Skyrme MDI in Fig. 1 as the red line. The values of b_l, \tilde{C}_0 , and \tilde{D}_0 for $N = 4, 5$, and 6 are listed in Table I. Our calculations show that the results of the EOS, single-particle potential, and

TABLE I. The parameters of b_l used in extended Skyrme MDI are in GeV^{2-2l} and \tilde{C}_0, \tilde{D}_0 are fm^3/GeV .

N	b_0	b_1	b_2	b_3	b_4	b_5	b_6	\tilde{C}_0	\tilde{D}_0
4	-1.105	3.649	-2.608	0.826	-0.093	-	-	0.182	0.00
5	-1.135	4.137	-3.821	1.837	-0.428	0.038	-	0.182	0.00
6	-1.149	4.434	-4.828	3.048	-1.070	0.193	-0.014	0.182	0.00

HIC observables are independent of the N we used, since they are used to fit the same data. In the following calculations, we keep $N = 4$ and the values of b_1 to b_4 are fixed. Nevertheless, the extrapolated strength of the single-particle potential above 1 GeV is different for different N , and which should be investigated by using the HICs at high beam energies [61] and will not be discussed in this paper.

B. Single-particle potential, equation of state, and symmetry energy

Now let us check the neutron and proton single-particle potentials and the isospin asymmetric nuclear equation of state obtained with the extended Skyrme MDI. For comparison, we also plot the corresponding results obtained with the standard Skyrme MDI. In the calculations, we fix the values of $K_0 = 230$ MeV, $m_s^*/m = 0.77$, $S_0 = 32$ MeV, and vary the L and the f_I . In Table II, we list the corresponding interaction parameters, such as α , β , γ , A_{sym} , B_{sym} , \tilde{C}_0 , and \tilde{D}_0 , that will be used in the transport models. The values in brackets from the second to the eighth rows represent the values obtained with the standard Skyrme MDI as in Ref. [15].

Since the isospin asymmetric nuclear equation of state can be written as,

$$E(\rho, \delta)/A = E_0(\rho, \delta = 0)/A + S(\rho)\delta^2 + \dots, \quad (41)$$

with a parabolic approximation, the isospin symmetric part of EOS $E(\rho, \delta = 0)/A$ is presented in Fig. 2(a) and the density dependence of symmetry energy $S(\rho)$ is presented in Fig. 2(b). The gray lines in Fig. 2(a) are the EOS obtained by the 123 standard Skyrme interaction sets. It shows that the extended Skyrme interaction can reasonably reproduce the EOS for symmetric nuclear matter, and avoid the defect of describing EOS by only using the Taylor expansion parameters as described in Ref. [62].

Figure 2(b) is the density dependence of the symmetry energy obtained with the extended Skyrme MDI (colored lines)

and the standard Skyrme MDI (gray lines). As expected, the results obtained with different L exhibit different density dependence of the symmetry energy. However, the influence of different f_I on the density dependence of the symmetry energy is weak. For the standard Skyrme MDI (gray lines), the influence of different f_I mainly appears at the density above $1.5\rho_0$. At $\rho = 2\rho_0$, the difference between the symmetry energy obtained with two f_I is less than 7% for $L = 100$ MeV, and is less than 13% for $L = 46$ MeV. For extended Skyrme MDI, the density dependence of the symmetry energy obtained with $f_I = 0.3$ (solid lines) and $f_I = -0.3$ (dashed lines) are close to each other at both $L = 46$ or 100 MeV at $\rho < 3\rho_0$. The reason is that the different effective mass splitting obtained by the extended Skyrme MDI have a smaller impact on the A_{sym} , B_{sym} , and $C_{\text{sym}}^{(l)}$ terms in the density dependent of the symmetry energy compared with the standard Skyrme MDI according to Eqs. (33)–(35).

Based on the above discussions, one can expect the symmetry energy constraints from the properties of the neutron stars, such as the mass-radius relationship and the tidal deformability, cannot well distinguish f_I (or effective-mass splitting Δm_{np}^*), because the Tolman-Oppenheimer-Volkov (TOV) equation of neutron stars only depends on the pressure vs density [63]. However, the similar density-dependent symmetry energy from different f_I could lead to different effects on the HICs observables via the momentum-dependent symmetry potential, and thus the constraints of the symmetry energy from HICs may be different from the constraints from neutron stars.

To see the neutron and proton single-particle potentials (V_n and V_p) in isospin asymmetric nuclear matter obtained with different f_I (or effective mass splitting), we present the V_n and V_p as functions of kinetic energies in nuclear matter with $\delta = 0.2$ in Fig. 3. The upper panels, middle panels, and bottom panels are the results obtained at the densities $\rho = 0.3\rho_0$, ρ_0 , and $1.5\rho_0$, respectively. Figures 3(a)–3(c) present the neutron potential V_n (black lines) with $f_I = +0.3$, and Figs. 3(d)–3(f)

TABLE II. The parameters used in the calculations corresponding to $K_0 = 230$ MeV, $m_s^*/m = 0.77$, $S_0 = 32$ MeV, and different values of L and f_I . The parameters α , β , A_{sym} , B_{sym} are in MeV. \tilde{C}_0 and \tilde{D}_0 are fm^3/GeV .

Para.	$(L = 46, f_I = 0.3)$	$(L = 46, f_I = -0.3)$	$(L = 100, f_I = 0.3)$	$(L = 100, f_I = -0.3)$
α		-236.58 (-265.78)		
β		163.95 (194.93)		
γ		1.26 (1.22)		
A_{sym}	83.65 (108.44)	58.57 (62.73)	14.41 (25.32)	-10.67 (-20.40)
B_{sym}	-79.48 (-103.69)	-30.52 (-35.38)	-10.25 (-20.34)	38.72 (47.96)
\tilde{C}_0	-7.92×10^{-4} (-2.08×10^{-3})	0.37 (1.00)	-7.92×10^{-4} (-2.08×10^{-3})	0.37 (1.00)
\tilde{D}_0	0.37 (1.00)	-0.37 (-1.00)	0.37 (1.00)	-0.37 (-1.00)

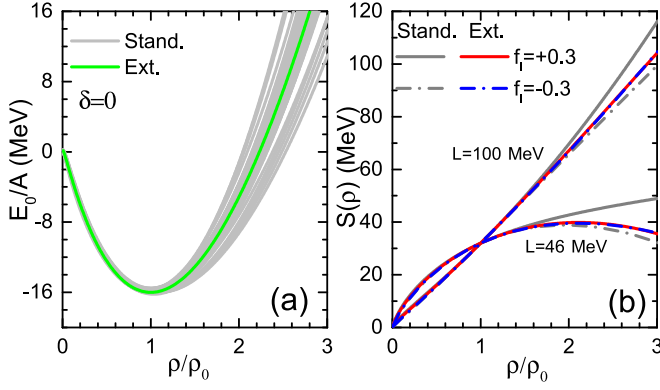


FIG. 2. (a) The equation of state obtained with the extended Skyrme MDI and the standard Skyrme MDI. (b) The density dependence of the symmetry energy obtained with the extended Skyrme MDI and the standard Skyrme MDI at $f_I = \pm 0.3$ and $L = 46, 100$ MeV.

are the proton potential V_p (red lines) with $f_I = -0.3$. All these results are obtained according to the Eqs. (15)–(17). The dashed lines are obtained with the standard Skyrme MDI, and the solid lines are obtained with the extended Skyrme MDI.

As expected, the values of V_n and V_p obtained from the extended Skyrme MDI reach an asymptotic value with an increase of E_k at densities we presented. Generally, the strength of single-particle potential increases with the density increasing, and similar trends are for the strength of symmetry potential. There is a cross point of symmetry potential obtained with $f_I = 0.3$ and $f_I = -0.3$, and this point moves to a high kinetic energy region with the density increasing. This behavior can be observed by the energy spectral of neutron-to-proton yield ratios, i.e., $R_{n/p}$, as discussed in our previous published results [27].

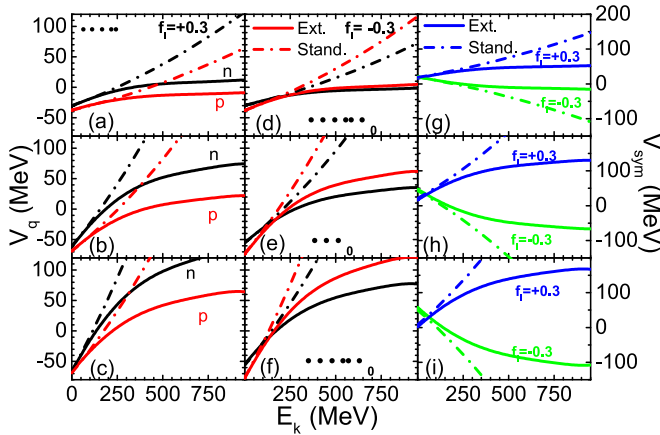


FIG. 3. Left panels and middle panels are the single-particle potential for $f_I = 0.3$ and $f_I = -0.3$, respectively. Right panels are the symmetry potential. The upper, middle, and bottom panels are the results at $\rho = 0.3\rho_0$, $\rho = \rho_0$ and $\rho = 1.5\rho_0$. Solid lines are the results obtained with extended MDI, and dashed lines are for standard Skyrme MDI.

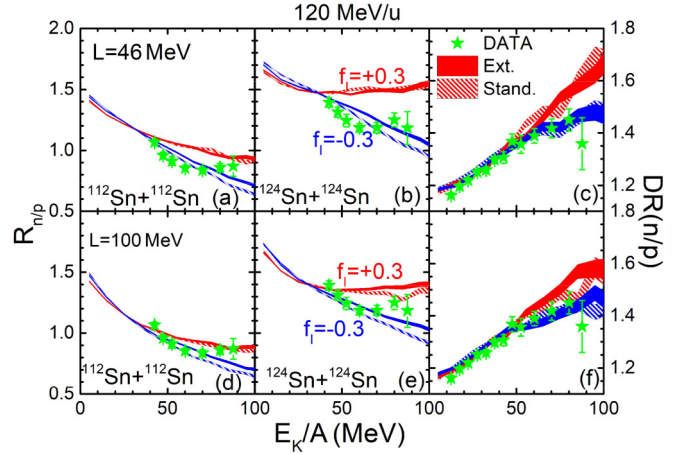


FIG. 4. $R_{n/p}$ and $DR(n/p)$ as a function of E_k/A at the beam energy $E_{\text{beam}} = 120$ MeV/u in the transverse direction $70^\circ \leq \theta_{\text{c.m.}} \leq 110^\circ$.

Focusing on the impact of f_I , one can observe that the V_n is greater than V_p when $f_I = 0.3$ ($m_n^* < m_p^*$). In more detail, neutrons will feel a stronger repulsive force than protons at high kinetic energy where $V_q > 0$, and neutrons feel a weaker attractive force than protons at low kinetic energy where $V_q < 0$. For $f_I = -0.3$ ($m_n^* > m_p^*$), V_n is less than V_p at $E_k > 150$ MeV and a contradictory behavior is observed at $E_k < 150$ MeV. To single out the contributions from the isoscalar single-particle potential, the symmetry potentials V_{sym} as functions of kinetic energy E_k are plotted in Figs. 3(g)–3(i). The convention of the line styles is as same as in Figs. 3(a)–3(f). The green and blue lines represent $f_I = -0.3$ and $f_I = +0.3$, respectively. The V_{sym} increases (decreases) with the kinetic energy increasing for $f_I = +0.3$ ($f_I = -0.3$). Different than the standard Skyrme MDI, the values of V_{sym} obtained from the extended Skyrme MDI tend to flatten out as E_k increases. Thus, one may expect the difference of the neutron to proton yield ratios in HICs, i.e., $Y(n)/Y(p)$, obtained from two different f_I will become smaller for the extended Skyrme MDI than that for standard Skyrme interaction.

C. The effects of extended Skyrme momentum-dependent interaction on the neutron-to-proton ratios

To see the influence by using the extended Skyrme MDI and the standard Skyrme MDI on the HICs observables, the central collisions of the systems $A = {}^{124}\text{Sn} + {}^{124}\text{Sn}$ and $B = {}^{112}\text{Sn} + {}^{112}\text{Sn}$ are simulated at the beam energy of 120 MeV/u and $b = 2$ fm. The HIC observables, i.e., the single ratio of the coalescence invariant (CI) neutron and proton $R_{n/p} = Y_{\text{CI}}(n)/Y_{\text{CI}}(p)$ and the double ratio of the coalescence invariant (CI) neutron and proton $DR(n/p) = R_{n/p}(A)/R_{n/p}(B)$, are analyzed under different L and f_I . The $Y_{\text{CI}}(n)$ and $Y_{\text{CI}}(p)$ are obtained by combining the free nucleons with those bound in light isotopes with $1 < A < 5$ [58,64].

In Fig. 4, we present the $R_{n/p}$ and $DR(n/p)$ as a function of E_k/A , i.e., the kinetic energy per nucleon of emitted particles in the center of mass frame at the beam energy $E_{\text{beam}} = 120$ MeV/u. The left and middle panels are $R_{n/p}$ for

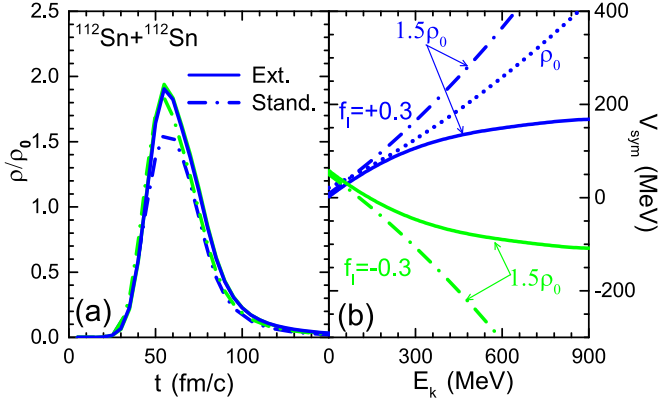


FIG. 5. Panel (a) is time evolution of average density in center of system. Panel (b) is the symmetry potential for $f_I = 0.3$ and $f_I = -0.3$ at different densities.

$^{112}\text{Sn} + ^{112}\text{Sn}$ and $^{124}\text{Sn} + ^{124}\text{Sn}$, respectively. The right panels are for the $DR(n/p)$. Our calculations show that the values of $R_{n/p}$ and $DR(n/p)$ obtained with $f_I = 0.3$ are greater than that with $f_I = -0.3$ at high kinetic energy region for both MDIs (shaded regions) and both L (the results for $L = 46$ MeV are in the upper panels and the results for $L = 100$ MeV are in the bottom panels). It can be understood from the symmetry potential presented in Fig. 3.

Another, to understand the difference of the $R_{n/p}$ [or $DR(n/p)$] obtained with two MDIs, we also present the results obtained with standard Skyrme MDI in the dashed shaded regions. The values of $R_{n/p}$ obtained with the extended Skyrme-type MDI are almost the same as those obtained with the standard Skyrme MDI in the low kinetic energy region where the symmetry potential of the two MDI forms is basically the same. At the high kinetic energy region, the $R_{n/p}$ obtained with the extended Skyrme MDI is different than that with standard Skyrme MDI, but the difference depends on the f_I . In the case of $f_I = -0.3$, the $R_{n/p}$ obtained with extended Skyrme MDI are obviously larger than that with standard Skyrme MDI. But for $f_I = 0.3$, the $R_{n/p}$ obtained with extended Skyrme MDI are close to that with standard Skyrme MDI. It seems contradictory with the symmetry potential presented in Fig. 3 but can be understood from the reaction dynamics.

In the simulations of HICs, the maximum compressed density depends on the form of MDI, as shown in Fig. 5(a). For $f_I = -0.3$, our calculations show that the maximum compressed density reaches about $1.94\rho_0$ for extended Skyrme MDI and reaches about $1.84\rho_0$ for standard Skyrme MDI. The difference of the maximum compressed density obtained with two MDIs is less than 6%. Thus, the difference of $R_{n/p}$ obtained with two MDIs will be similar with the difference of symmetry potential at a certain density. However, for $f_I = 0.3$, the difference of the maximum compressed density obtained with two MDIs reaches about 18%, where the maximum compressed density reaches about $1.9\rho_0$ for extended Skyrme MDI and reaches about $1.56\rho_0$ for standard Skyrme MDI. Consequently, the difference of $R_{n/p}$ obtained with two MDIs will not be similar with the difference of symmetry

potential at a certain density. It will be like a difference of the symmetry potential at two densities for two MDIs. For example, as shown in Fig. 5(b), the difference of the symmetry potential obtained with the extended Skyrme MDI at $1.5\rho_0$ and the symmetry potential obtained with the standard Skyrme MDI at $1.0\rho_0$ is small, and thus the difference of $R_{n/p}$ between two MDIs becomes smaller for $f_I = 0.3$.

The differences of the single-particle potential between the extended Skyrme MDI and standard MDI become obvious at higher beam energies. Therefore, the $R_{n/p}$ and $DR(n/p)$ at the beam energies of 270 and 400 MeV/u, which is in the capability of ImQMD model, are also analyzed. The calculated results are presented in Fig. 6. Similar to the results at 120 MeV/u, the $R_{n/p}$ and $DR(n/p)$ obtained with $f_I = 0.3$ are greater than that with $f_I = -0.3$ in the high kinetic energy region. To quantitatively describe the isospin effective-mass splitting effects on $R_{n/p}$, we construct the difference of $R_{n/p}$ between two kinds of f_I , i.e.,

$$\Delta R_{n/p} = R_{n/p}(f_I = +0.3) - R_{n/p}(f_I = -0.3). \quad (42)$$

Our calculations reveal that $\Delta R_{n/p}$ obtained with the extended Skyrme MDI is smaller than that with standard Skyrme MDI, and this difference increases with the beam energy. For example, for $^{124}\text{Sn} + ^{124}\text{Sn}$, the difference of $\Delta R_{n/p}$ between the extended Skyrme MDI and standard Skyrme MDI increases from 15% to 45% at $E_k/E_{\text{beam}} = 0.75$ as the beam energy increases from 120 to 400 MeV/u.

D. Discussions on the constraints of the effective mass splitting

Furthermore, we also compare the calculation to the corrected data of $R_{n/p}$ and $DR(n/p)$ (green symbols) that were published in Ref. [58]. In general, the calculated $R_{n/p}$ and $DR_{n/p}$ obtained with $f_I = -0.3$ ($\Delta m_{np}^* \approx 0.311\delta$) are close to the data points for $L = 46$ MeV. In the case of $L = 100$ MeV, the data fall into the middle between the results obtained with $f_I = -0.3$ ($\Delta m_{np}^* \approx 0.311\delta$) and $f_I = 0.3$ ($\Delta m_{np}^* \approx -0.311\delta$). It implies that the Δm_{np}^* is negatively correlated with L , which is consistent with the results obtained with Hugenholtz-Van Hove (HVH) theorem [65]. This conclusion is consistent with the previous results in Ref. [58]. However, one should note that the $DR(n/p)$ suppresses the sensitivity to effective mass splitting, and the curves of $R_{n/p}$ as a function of E_k are different from the data for both reaction systems if we carefully check its shape. Therefore, it is important to further quantitatively analyze the shapes of $R_{n/p}$ as a function of E_k .

To probe the strength of the effective-mass splitting which only depends on the momentum-dependent part of the symmetry potential [as mentioned in Eq. (28)], one has to single out the contributions from the momentum-dependent part of the symmetry potential. The slope of $\ln R_{n/p}$ as a function of E_k/A , i.e.,

$$S_{n/p} = \frac{\partial \ln R_{n/p}}{\partial E_k/A}, \quad (43)$$

can be used as mentioned in Ref. [33]. According to the statistical and dynamical model [66–71], the neutron-to-proton

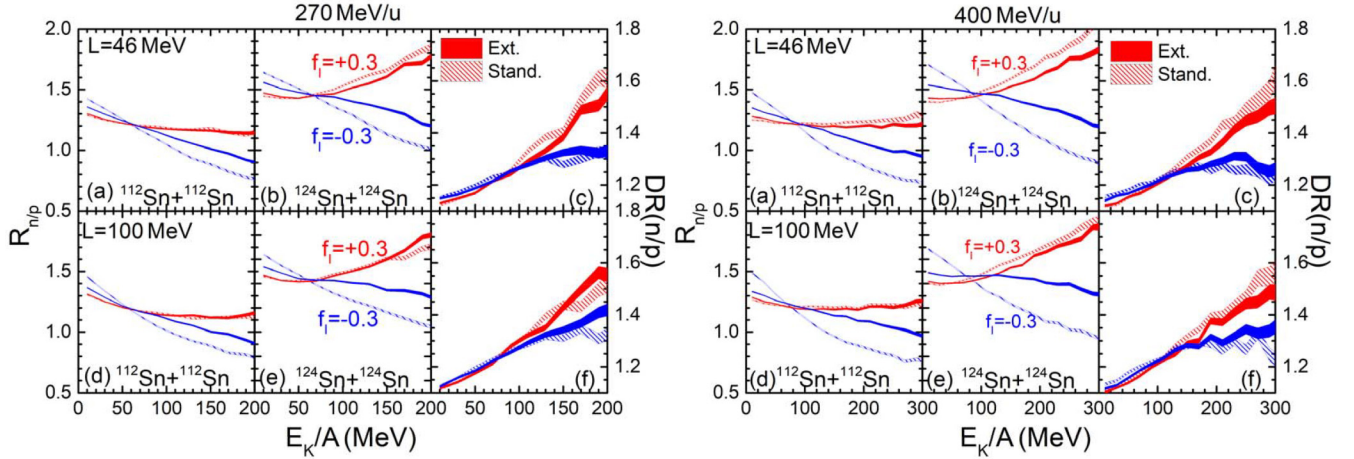


FIG. 6. The $R_{n/p}$ and $DR(n/p)$ as a function of E_k/A at the beam energy $E_{\text{beam}} = 270 \text{ MeV/u}$, 400 MeV/u in transverse direction $70^\circ \leq \theta_{\text{c.m.}} \leq 110^\circ$.

yield ratios $R_{n/p}$ can be written as

$$R_{n/p} = \frac{Y(n)}{Y(p)} \propto \exp\left(\frac{\mu_n - \mu_p}{T}\right) = \exp\left(\frac{2V_{\text{sym}}\delta}{T}\right). \quad (44)$$

T is the temperature of the emitting source, μ_n and μ_p are the chemical potentials of neutrons and protons, respectively. If we expand the symmetry potential with respect to p^2 , i.e., $V_{\text{sym}} = V_{\text{sym}}^0 + \frac{\partial V_{\text{sym}}}{\partial p^2} p^2 + \dots$, then $R_{n/p}$ can be written as

$$R_{n/p} \propto \exp\left[\frac{2\left(V_{\text{sym}}^0 + \frac{\partial V_{\text{sym}}}{\partial p^2} p^2 + \dots\right)\delta}{T}\right] \approx \exp\left[\frac{2V_{\text{sym}}^0\delta}{T}\right] \exp\left[-\frac{\left(\frac{m}{m^*}\right)^2 \Delta m_{np}^* E'_k}{T}\right]. \quad (45)$$

$E'_k = p_{\text{rel}}^2/2m$ is the relative kinetic energy between colliding nucleon pairs during the collisions, which should positively correlate to the kinetic energy of emitted nucleons. If we simply assume $E'_k = \lambda E_k/A$, then we have

$$S_{n/p} = -\frac{\lambda}{T} \left(\frac{m}{m^*}\right)^2 \Delta m_{np}^*, \quad (46)$$

which is directly related to the Δm_{np}^* . If one assumes $\lambda = 1$ and $T = 5 \text{ MeV}$, the estimated values of $S_{n/p}$ are in the range from ± 0.02 for the parameters we used, i.e., $m_s^*/m = 0.77$ and $f_I = \pm 0.3$. In the HICs, the λ is related to the friction of the system and the value should be smaller than one. Thus, one can expect $|S_{n/p}| < 0.02$ if $T = 5 \text{ MeV}$.

In Fig. 7, we present the $S_{n/p}$ obtained in the simulation and data. Two kinetic regions, i.e., the kinetic energy per nucleon of the emitted particles in the range of $35 \text{ MeV} \leq \Delta E_1 \leq 55 \text{ MeV}$ and $55 \text{ MeV} \leq \Delta E_2 \leq 95 \text{ MeV}$, are used to calculate $S_{n/p}$. The systems of $^{112}\text{Sn} + ^{112}\text{Sn}$ and $^{124}\text{Sn} + ^{124}\text{Sn}$ at the beam energy of 120 MeV/u are presented in the left and right panels, respectively. The red circles represent the results obtained with $f_I = 0.3$, the blue circles represent the results with $f_I = -0.3$. The green squares are the data points of $S_{n/p}$ which are extracted from the published experimental

data [58]. One can find that the calculations tend to favor different effective mass splitting at different kinetic energy regions. In quality, the calculated values of $S_{n/p}$ tend to favor $f_I < 0$ ($m_n^* > m_p^*$) at the kinetic energy less than 55 MeV . At the kinetic energy greater than 55 MeV , the calculated values of $S_{n/p}$ tend to favor $f_I > 0$ ($m_n^* < m_p^*$). It implies the $m_n^* > m_p^*$ at low kinetic energy and $m_n^* < m_p^*$ at high kinetic energy, which is consistent with the theoretical calculations from the relativistic Hartree-Fock calculations [72]. In quantity, the calculations cannot exactly describe the shape of $R_{n/p}$ by the parameter sets we used. The possible reasons may be a reasonable parameter set is not used or the cluster formation for light particles is not well described. To rule out the first reason, a systematic analysis of $R_{n/p}$ on the multidimensional parameter space is certainly needed before going to understand the cluster formation mechanism and draw a firm conclusion on the effective mass splitting.

In addition, the uncertainties of the transport models should also be investigated in future studies. Generally, the

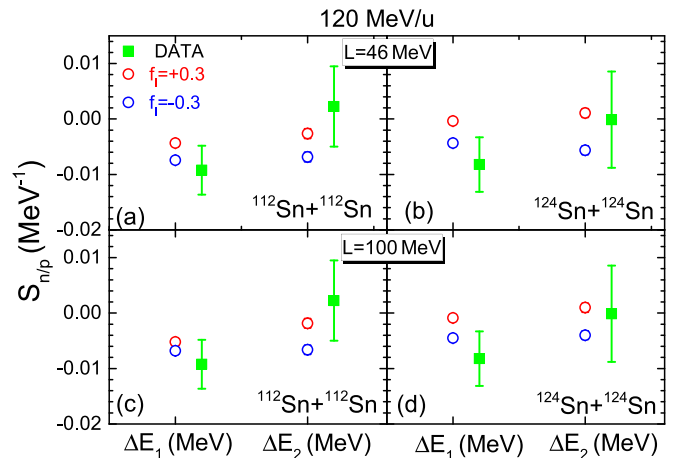


FIG. 7. $S_{n/p}$ at two kinetic regions and at beam energy $E_{\text{beam}} = 120 \text{ MeV/u}$ in the transverse direction $70^\circ \leq \theta_{\text{c.m.}} \leq 110^\circ$. Data points are extracted from the published $R_{n/p}$ in Ref. [58].

uncertainty of the transport models arises from three aspects. One is from the numerical techniques, and another is from the uncertainty of the physical quantities. The third one is from the systematic uncertainties due to the missed physics. The first point has stimulated the transport model evaluation project (TMEP) to improve the transport model. There are some important progresses have been made in the mean-field part [73], nucleon-nucleon collision part [74,75], and recent progress is available in Ref. [17]. The second point has led to the application of the Bayesian analysis on the heavy ion collision observables in multidimensional parameter space, as in Refs. [15,58]. One should notice that the new form of the extended MDI may influence the in-medium nucleon-nucleon cross sections from the point view of both mean-field and the in-medium nucleon-nucleon cross sections in the transport equation have the same origin. When the in-medium nucleon-nucleon cross sections are modified in the transport model, the values of $R_{n/p}$ may be further modified except for the impacts from the mean-field potential. Nonetheless, the results in Ref. [76] suggest that the medium correction on the nucleon-nucleon cross sections weakly influences the $R_{n/p}$ since it is mainly determined by the strength of symmetry energy. To quantitatively estimate the uncertainty of this medium correction of the nucleon-nucleon cross sections on $R_{n/p}$, a Bayesian analysis of the heavy ion collisions observables in multidimensional parameter space, which includes the degree of the medium corrections on the nucleon-nucleon cross sections, is needed. The third one comes from the philosophy of solving the many-body transport equations and missed physics, which will be an important point to develop an advanced model for describing the complex collisions as wished in the long-range plan of nuclear science [77].

IV. SUMMARY

The main goal of this work is to obtain an extended Skyrme momentum-dependent interaction, and its related mean-field potential and Hamiltonian. The forms we provided have the following properties: First, the extended Skyrme MDI extends the utility of the effective Skyrme interaction to a wider energy region in the transport models. For instance, this form can be used to calculate the vector potential and scalar potential for studying the effects of the effective mass splitting and the isospin-dependent threshold of the pion production for HICs below 1 GeV/u, as in Ref. [32]. Second, the effect of the width of the wave packet can be explicitly involved in the MDI part of the QMD-type Hamiltonian. Third, this form can be easily used in both the BUU and QMD-type models for simulating

the heavy ion collisions at intermediate to high energies. In another, the relationship between the nuclear matter parameters and the interaction parameters used in the transport models are provided, which makes the transport model investigate the nuclear matter parameter in multidimensional parameter space easily.

As an example of the application of the extended Skyrme MDI, we incorporate the extended Skyrme MDI into the ImQMD model. The isospin sensitive observables, such as the single and double ratios of the coalescence neutron to proton yields [$R_{n/p}$ and $DR(n/p)$] for $^{112,124}\text{Sn} + ^{112,124}\text{Sn}$ at the beam energy of 120, 270, and 400 MeV/u are analyzed to understand the influence of effective mass splitting. Our calculations show that the difference of the $R_{n/p}$ ratios obtained with two different strengths of the effective mass splitting, i.e., $f_I = +0.3$ and $f_I = -0.3$, becomes weaker for the extended Skyrme MDI than that for the standard Skyrme MDI.

Finally, we also propose a probe for constraining the strength of the effective mass splitting, i.e., the slope of $\ln R_{n/p}$ as a function of E_k/A ,

$$S_{n/p} = \frac{\partial \ln R_{n/p}}{\partial E_k/A}.$$

Our calculations show that $S_{n/p}$ is directly related to the effective mass splitting Δm_n^* . By comparing $S_{n/p}$ with the experimental data, in quality, one can find that the calculations favor different effective mass splitting at different kinetic energy regions. The calculated values of $S_{n/p}$ tend to favor $m_n^* > m_p^*$ at the kinetic energy less than 55 MeV and tend to favor $m_n^* < m_p^*$ at the kinetic energy greater than 55 MeV. In quantity, the calculations cannot accurately describe the shape of $R_{n/p}$ by the parameter sets we used. Thus, further analysis on the $R_{n/p}$ in multidimensional parameter space is certainly needed to understand the discrepancy and to reliably constrain the effective mass splitting.

ACKNOWLEDGMENTS

This work was partly inspired by the transport model evaluation project and was supported by the National Natural Science Foundation of China under Grants No. 12275359, No. 12375129, No. 11875323, and No. 11961141003, by the National Key R&D Program of China under Grant No. 2023 YFA1606402, by the Continuous Basic Scientific Research Project, by funding of the China Institute of Atomic Energy under Grant No. YZ222407001301, No. YZ232604001601, and by the Leading Innovation Project of the CNNC under Grants No. LC192209000701 and No. LC202309000201.

APPENDIX A: ENERGY DENSITY OF THE EXTENDED SKYRME-TYPE MOMENTUM-DEPENDENT INTERACTION

The extended Skyrme-type MDI energy density is

$$u_{md} = \tilde{C}_0 \int d^3p d^3p' f(\mathbf{r}, \mathbf{p}) f(\mathbf{r}, \mathbf{p}') g(\mathbf{p} - \mathbf{p}') + \tilde{D}_0 \int d^3p d^3p' f_n(\mathbf{r}, \mathbf{p}) f_n(\mathbf{r}, \mathbf{p}') g(\mathbf{p} - \mathbf{p}') \\ + \tilde{D}_0 \int d^3p d^3p' f_p(\mathbf{r}, \mathbf{p}) f_p(\mathbf{r}, \mathbf{p}') g(\mathbf{p} - \mathbf{p}').$$

$$\begin{aligned}
 &= \tilde{C}_0 \int d^3 p d^3 p' (f_n(\mathbf{r}, \mathbf{p}) f_n(\mathbf{r}, \mathbf{p}') + f_n(\mathbf{r}, \mathbf{p}) f_p(\mathbf{r}, \mathbf{p}') + f_p(\mathbf{r}, \mathbf{p}) f_n(\mathbf{r}, \mathbf{p}') + f_p(\mathbf{r}, \mathbf{p}) f_p(\mathbf{r}, \mathbf{p}')) g(\mathbf{p} - \mathbf{p}') \\
 &+ \tilde{D}_0 \int d^3 p d^3 p' f_n(\mathbf{r}, \mathbf{p}) f_n(\mathbf{r}, \mathbf{p}') g(\mathbf{p} - \mathbf{p}') + \tilde{D}_0 \int d^3 p d^3 p' f_p(\mathbf{r}, \mathbf{p}) f_p(\mathbf{r}, \mathbf{p}') g(\mathbf{p} - \mathbf{p}').
 \end{aligned} \tag{A1}$$

$g(\mathbf{p} - \mathbf{p}')$ is taken as

$$\begin{aligned}
 g(\mathbf{p} - \mathbf{p}') &= b_0 + b_1(\mathbf{p} - \mathbf{p}')^2 + b_2(\mathbf{p} - \mathbf{p}')^4 + b_3(\mathbf{p} - \mathbf{p}')^6 + b_4(\mathbf{p} - \mathbf{p}')^8 \\
 &= \sum_{l=0}^{N=4} b_l \left[\sum_{l=0, \in \text{even}}^{2l} \binom{2l}{l} p^l (-p')^{2l-l} - \sum_{l=1, \in \text{odd}}^{2l} \binom{2l}{l} p^{l-1} (-p')^{2l-l-1} \mathbf{p} \cdot \mathbf{p}' \right].
 \end{aligned} \tag{A2}$$

For cold uniform nuclear matter, $f_q = \frac{2}{(2\pi\hbar)^3} \Theta(p_{F_q} - p)$, $q = n/p$, and an analytical expression of u_{md} can be obtained.

For the \tilde{C}_0 term,

$$\begin{aligned}
 &\tilde{C}_0 \int d^3 p d^3 p' [f_n(\mathbf{r}, \mathbf{p}) f_n(\mathbf{r}, \mathbf{p}') + f_n(\mathbf{r}, \mathbf{p}) f_p(\mathbf{r}, \mathbf{p}') + f_p(\mathbf{r}, \mathbf{p}) f_n(\mathbf{r}, \mathbf{p}') + f_p(\mathbf{r}, \mathbf{p}) f_p(\mathbf{r}, \mathbf{p}')] g(\mathbf{p} - \mathbf{p}') \\
 &= \tilde{C}_0 \left(\frac{2}{(2\pi\hbar)^3} \right)^2 \left(\int_0^{p_{F_n}} d\mathbf{p} \int_0^{p_{F_n}} d\mathbf{p}' + \int_0^{p_{F_n}} d\mathbf{p} \int_0^{p_{F_p}} d\mathbf{p}' + \int_0^{p_{F_p}} d\mathbf{p} \int_0^{p_{F_n}} d\mathbf{p}' + \int_0^{p_{F_p}} d\mathbf{p} \int_0^{p_{F_p}} d\mathbf{p}' \right) \\
 &\times \sum_{l=0}^4 b_l \left[\sum_{l=0, \in \text{even}}^{2l} \binom{2l}{l} p^l (-p')^{2l-l} - \sum_{l=1, \in \text{odd}}^{2l} \binom{2l}{l} p^{l-1} (-p')^{2l-l-1} \mathbf{p} \cdot \mathbf{p}' \right].
 \end{aligned} \tag{A3}$$

Since the terms with l equal to an odd number are zero, the \tilde{C}_0 term will be

$$\begin{aligned}
 &= \tilde{C}_0 \left(\frac{2}{(2\pi\hbar)^3} \right)^2 (4\pi)^2 \left[\sum_{l=0}^N b_l \sum_{l=0, l \in \text{even}}^{2l} \binom{2l}{l} \left(\int_0^{p_{F_n}} p^{2+l} dp \int_0^{p_{F_n}} p^{2+2l-l} dp' + \int_0^{p_{F_n}} p^{2+l} dp \right. \right. \\
 &\quad \left. \left. \times \int_0^{p_{F_p}} p^{2+2l-l} dp' + \int_0^{p_{F_p}} p^{2+l} dp \int_0^{p_{F_n}} p^{2+2l-l} dp' + \int_0^{p_{F_p}} p^{2+l} dp \int_0^{p_{F_p}} p^{2+2l-l} dp' \right) \right] \\
 &= \tilde{C}_0 \left(\frac{2}{(2\pi\hbar)^3} \right)^2 (4\pi)^2 \left[\sum_{l=0}^N b_l \sum_{l=0, l \in \text{even}}^{2l} \binom{2l}{l} \frac{1}{(l+3)} \frac{1}{(2l-l+3)} \right. \\
 &\quad \left. \times (p_{F_n}^{l+3} p_{F_n}^{2l-l+3} + p_{F_n}^{l+3} p_{F_p}^{2l-l+3} + p_{F_p}^{l+3} p_{F_n}^{2l-l+3} + p_{F_p}^{l+3} p_{F_p}^{2l-l+3}) \right] \\
 &= \tilde{C}_0 \left[\sum_{l=0}^N b_l \sum_{l=0, l \in \text{even}}^{2l} \mathcal{G}_{ll} \sum_{q, q'} \rho_q^{(l+3)/3} \rho_{q'}^{(2l-l+3)/3} \right].
 \end{aligned} \tag{A4}$$

Here

$$\mathcal{G}_{lk} = \left(\frac{2}{(2\pi\hbar)^3} \right)^2 (4\pi)^2 \left\{ [\hbar(3\pi^2)^{1/3}]^{(2l+6)} \binom{2l}{l} \frac{1}{(l+3)} \frac{1}{(2l-l+3)} \right\},$$

and $p_{F_q} = \hbar(3\pi^2 \rho_q)^{1/3}$.

Similarly, the \tilde{D}_0 terms

$$\begin{aligned}
 \tilde{D}_0 \int d^3 p d^3 p' f_q(\mathbf{r}, \mathbf{p}) f_q(\mathbf{r}, \mathbf{p}') g(\mathbf{p} - \mathbf{p}') &= \tilde{D}_0 \left(\frac{2}{(2\pi\hbar)^3} \right)^2 (4\pi)^2 \int_0^{p_{F_q}} p^2 dp \int_0^{p_{F_q}} p'^2 dp' \left[\sum_{l=0}^N b_l \sum_{l=0, l \in \text{even}}^{2l} \binom{2l}{l} p^l (-p')^{2l-l} \right] \\
 &= \tilde{D}_0 \left(\frac{2}{(2\pi\hbar)^3} \right)^2 (4\pi)^2 \left[\sum_{l=0}^N b_l \sum_{l=0, l \in \text{even}}^{2l} \binom{2l}{l} \frac{1}{(l+3)} \frac{1}{(2l-l+3)} p_{F_q}^{2l+6} \right] \\
 &= \tilde{D}_0 \left[\sum_{l=0}^N b_l \sum_{l=0, l \in \text{even}}^{2l} \mathcal{G}_{ll} \rho_q^{(2l+6)/3} \right].
 \end{aligned} \tag{A5}$$

u_{md} will be

$$u_{md} = \tilde{C}_0 \left[\sum_{l=0}^N b_l \sum_{l=0, l \in \text{even}}^{2l} \mathcal{G}_{ll} \sum_{q, q'} \rho_q^{(l+3)/3} \rho_{q'}^{(2l-l+3)/3} \right] + \tilde{D}_0 \left[\sum_{l=0}^N b_l \sum_{l=0, l \in \text{even}}^{2l} \mathcal{G}_{ll} \sum_q \rho_q^{(2l+6)/3} \right]. \quad (\text{A6})$$

By using the relation $\rho_q = \frac{\rho}{2}(1 + \tau_q \delta)$, with $\tau_q = 1$ (-1) for neutrons (protons), the above equation can be rewritten as follows:

$$\begin{aligned} u_{md} &= \tilde{C}_0 \left[\sum_{l=0}^N b_l \sum_{l=0, l \in \text{even}}^{2l} \mathcal{G}_{ll} \left(\frac{\rho}{2}\right)^{(2l+6)/3} \sum_{q, q'} (1 + \tau_q \delta)^{(l+3)/3} (1 + \tau_{q'} \delta)^{(2l-l+3)/3} \right] \\ &\quad + \tilde{D}_0 \left[\sum_{l=0}^N b_l \sum_{l=0, l \in \text{even}}^{2l} \mathcal{G}_{ll} \left(\frac{\rho}{2}\right)^{(2l+6)/3} \sum_q (1 + \tau_q \delta)^{(2l+6)/3} \right] \\ &\approx \tilde{C}_0 \left[\sum_{l=0}^N b_l \sum_{l=0, l \in \text{even}}^{2l} \mathcal{G}_{ll} \left(\frac{\rho}{2}\right)^{(2l+6)/3} \sum_{q, q'} \left(1 + \frac{l+3}{3} \tau_q \delta + \frac{1}{2} \frac{l+3}{3} \frac{l}{3} \delta^2\right) \right. \\ &\quad \left. \times \left(1 + \frac{(2l-l+3)}{3} \tau_{q'} \delta + \frac{1}{2} \frac{(2l-l+3)(2l-l)}{3} \delta^2\right) \right] \\ &\quad + \tilde{D}_0 \left[\sum_{l=0}^N b_l \sum_{l=0, l \in \text{even}}^{2l} \mathcal{G}_{ll} \left(\frac{\rho}{2}\right)^{(2l+6)/3} \sum_q \left(1 + \frac{2l+6}{3} \tau_q \delta + \frac{1}{2} \frac{2l+6}{3} \frac{2l+3}{3} \delta^2\right) \right]. \end{aligned} \quad (\text{A7})$$

With the parabolic approximation, the u_{md} can be rewritten as

$$u_{md} = u_{md}^0 + u_{md}^{\text{asy}} \delta^2 + \dots, \quad (\text{A8})$$

Thus, u_{md}^0 is

$$u_{md}^0 = 4 \left(\tilde{C}_0 + \frac{\tilde{D}_0}{2} \right) \left[\sum_{l=0}^N b_l \sum_{l=0, l \in \text{even}}^{2l} \mathcal{G}_{ll} \left(\frac{\rho}{2}\right)^{(2l+6)/3} \right]. \quad (\text{A9})$$

The asymmetry term u_{md}^{asy} is

$$\begin{aligned} u_{md}^{\text{asy}} &= 2\tilde{C}_0 \left[\sum_{l=0}^N b_l \sum_{l=0, l \in \text{even}}^{2l} \mathcal{G}_{ll} \left(\frac{\rho}{2}\right)^{(2l+6)/3} \left(\frac{l+3}{3} \frac{l}{3} + \frac{2l-l+3}{3} \frac{2l-l}{3} \right) \right] \\ &\quad + \tilde{D}_0 \left[\sum_{l=0}^N b_l \frac{2l+6}{3} \frac{2l+3}{3} \sum_{l=0, l \in \text{even}}^{2l} \mathcal{G}_{ll} \left(\frac{\rho}{2}\right)^{(2l+6)/3} \right]. \end{aligned} \quad (\text{A10})$$

APPENDIX B: SINGLE-PARTICLE POTENTIAL

The nonlocal part of single-particle potential of nucleon in cold uniform nuclear matter is

$$\begin{aligned} V_q^{\text{md}}(\rho, \delta, p) &= \frac{\delta u_{md}}{\delta f_q} = 2\tilde{C}_0 \int d^3 p' f(\mathbf{r}, \mathbf{p}') g(\mathbf{p} - \mathbf{p}') + 2\tilde{D}_0 \int_{\mathbf{p}' < p_{Fq}} d^3 p' f_q(\mathbf{r}, \mathbf{p}') g(\mathbf{p} - \mathbf{p}') \\ &= 2\tilde{C}_0 \sum_{\tau=n,p} \int_{\mathbf{p}' < p_{F\tau}} d^3 p' f_{\tau}(\mathbf{r}, \mathbf{p}') g(\mathbf{p} - \mathbf{p}') + 2\tilde{D}_0 \int_{\mathbf{p}' < p_{Fq}} d^3 p' f_q(\mathbf{r}, \mathbf{p}') g(\mathbf{p} - \mathbf{p}'). \end{aligned} \quad (\text{B1})$$

For the \tilde{C}_0 term,

$$\begin{aligned} 2\tilde{C}_0 \int d^3 p' f(\mathbf{r}, \mathbf{p}') g(\mathbf{p} - \mathbf{p}') &= 2\tilde{C}_0 \left(\frac{2}{(2\pi \hbar)^3} \right) 4\pi \left[\sum_{l=0}^N b_l \sum_{l=0, l \in \text{even}}^{2l} \binom{2l}{l} \frac{1}{(2l-l+3)} \left(p_{F_n}^{2l-l+3} + p_{F_p}^{2l-l+3} \right) p^l \right] \\ &= 2\tilde{C}_0 \left[\sum_{l=0}^N b_l \sum_{l=0, l \in \text{even}}^{2l} \tilde{\mathcal{A}}_{ll} \sum_q \rho_q^{(2l-l+3)/3} p^l \right], \end{aligned} \quad (\text{B2})$$

where

$$\tilde{\mathcal{A}}_{ll} = \frac{2}{(2\pi\hbar)^3} 4\pi \left\{ [\hbar(3\pi^2)^{1/3}]^{(2l-l+3)} \binom{2l}{l} \frac{1}{(2l-l+3)} \right\}.$$

Similarly, the \tilde{D}_0 terms are

$$\begin{aligned} 2\tilde{D}_0 \int d^3p' f_q(\mathbf{r}, \mathbf{p}') g(\mathbf{p} - \mathbf{p}') &= 2\tilde{D}_0 \left(\frac{2}{(2\pi\hbar)^3} \right) 4\pi \left[\sum_{l=0}^N b_l \sum_{l=0, l \in \text{even}}^{2l} \binom{2l}{l} \frac{1}{(2l-l+3)} p_{F_q}^{2l-l+3} p^l \right] \\ &= 2\tilde{D}_0 \left[\sum_{l=0}^N b_l \sum_{l=0, l \in \text{even}}^{2l} \tilde{\mathcal{A}}_{ll} \rho_q^{(2l-l+3)/3} p^l \right]. \end{aligned} \quad (\text{B3})$$

V_q^{md} will be

$$V_q^{\text{md}}(\rho, \delta, p) = 2\tilde{C}_0 \left[\sum_{l=0}^N b_l \sum_{l=0, l \in \text{even}}^{2l} \tilde{\mathcal{A}}_{ll} \sum_q \rho_q^{(2l-l+3)/3} p^l \right] + 2\tilde{D}_0 \left[\sum_{l=0}^N b_l \sum_{l=0, l \in \text{even}}^{2l} \tilde{\mathcal{A}}_{ll} \rho_q^{(2l-l+3)/3} p^l \right]. \quad (\text{B4})$$

By using the relation $\rho_q = \frac{\rho}{2}(1 + \tau_q \delta)$, with $\tau_q = 1$ or -1 for neutrons and protons, the above equation can be rewritten as follows:

$$\begin{aligned} V_q^{\text{md}}(\rho, \delta, p) &= 2\tilde{C}_0 \left[\sum_{l=0}^N b_l \sum_{l=0, l \in \text{even}}^{2l} \tilde{\mathcal{A}}_{ll} \left(\frac{\rho}{2} \right)^{(2l-l+3)/3} \sum_q (1 + \tau_q \delta)^{(2l-l+3)/3} p^l \right] \\ &\quad + 2\tilde{D}_0 \left[\sum_{l=0}^N b_l \sum_{l=0, l \in \text{even}}^{2l} \tilde{\mathcal{A}}_{ll} \left(\frac{\rho}{2} \right)^{(2l-l+3)/3} (1 + \tau_q \delta)^{(2l-l+3)/3} p^l \right] \\ &\approx 2\tilde{C}_0 \left[\sum_{l=0}^N b_l \sum_{l=0, l \in \text{even}}^{2l} \tilde{\mathcal{A}}_{ll} \left(\frac{\rho}{2} \right)^{(2l-l+3)/3} \sum_q \left(1 + \frac{2l-l+3}{3} \tau_q \delta + \dots \right) p^l \right] \\ &\quad + 2\tilde{D}_0 \left[\sum_{l=0}^N b_l \sum_{l=0, l \in \text{even}}^{2l} \tilde{\mathcal{A}}_{ll} \left(\frac{\rho}{2} \right)^{(2l-l+3)/3} \left(1 + \frac{2l-l+3}{3} \tau_q \delta + \dots \right) p^l \right]. \end{aligned} \quad (\text{B5})$$

V_{md} can be rewritten as

$$V_{md} = V_{md}^0 \pm V_{md}^{\text{sym}} \delta + \dots \quad (\text{B6})$$

Thus, V_{md}^0 is

$$V_{md}^0 = 4 \left(\tilde{C}_0 + \frac{\tilde{D}_0}{2} \right) \left[\sum_{l=0}^N b_l \sum_{l=0, l \in \text{even}}^{2l} \tilde{\mathcal{A}}_{ll} \left(\frac{\rho}{2} \right)^{(2l-l+3)/3} p^l \right]. \quad (\text{B7})$$

The asymmetry term V_{md}^{sym} is

$$V_{md}^{\text{sym}} = 2\tilde{D}_0 \left[\sum_{l=0}^N b_l \sum_{l=0, l \in \text{even}}^{2l} \tilde{\mathcal{A}}_{ll} \left(\frac{\rho}{2} \right)^{(2l-l+3)/3} \frac{2l-l+3}{3} p^l \right]. \quad (\text{B8})$$

APPENDIX C: RELATION BETWEEN THE EFFECTIVE MASS SPLITTING AND SYMMETRY POTENTIAL

According to Eq. (26),

$$\frac{m}{m_n^*} - \frac{m}{m_p^*} = 2m \left(\frac{\partial V_n}{\partial p^2} - \frac{\partial V_p}{\partial p^2} \right) = 4m\delta \frac{\partial V_{\text{sym}}}{\partial p^2}. \quad (\text{C1})$$

In addition,

$$\frac{m}{m_n^*} - \frac{m}{m_p^*} = -\frac{m(m_n^* - m_p^*)}{m_n^* m_p^*} \approx -\left(\frac{m}{m^*} \right)^2 \Delta m_{np}^*. \quad (\text{C2})$$

The approximation comes from $m_q^*/m = m^*/m \pm \delta m^*/m$, and the product

$$\frac{m_n^* m_p^*}{m^2} = \left(\frac{m^*}{m}\right)^2 - \left(\frac{\delta m^*}{m}\right)^2 \approx \left(\frac{m^*}{m}\right)^2.$$

APPENDIX D: HIGH-ORDER EXPANSION COEFFICIENTS OF NUCLEAR MATTER EQUATION OF STATE

Around the nuclear matter saturation density ρ_0 , the binding energy per nucleon in symmetric nuclear matter can be expanded (e.g., up to fourth order in density) as

$$E/A(\rho) = E_0(\rho_0) + \frac{K_0}{2!}x^2 + \frac{Q_0}{3!}x^3 + \frac{Z_0}{4!}x^4 + O(x^5), \quad (D1)$$

where x is a dimensionless variable, $x = (\rho - \rho_0)/3\rho_0$.

The incompressibility K_0 is

$$K_0 = 9\rho_0^2 \left. \frac{\partial^2 E/A}{\partial \rho^2} \right|_{\rho_0} = \frac{-6}{5}\epsilon_F^0 + 9\frac{\beta}{\gamma+1}\gamma(\gamma-1) + 6\left(\tilde{C}_0 + \frac{\tilde{D}_0}{2}\right) \sum_{I=1}^N \tilde{g}_{md}^{(I)} \left(\frac{2I}{3} + 1\right) I \rho_0^{2I/3+1}. \quad (D2)$$

The skewness coefficient Q_0 is

$$Q_0 = 27\rho_0^3 \left. \frac{\partial^3 E/A}{\partial \rho^3} \right|_{\rho_0} = \frac{24}{5}\epsilon_F^0 + 27\frac{\beta}{\gamma+1}\gamma(\gamma-1)(\gamma-2) + 27\left(\tilde{C}_0 + \frac{\tilde{D}_0}{2}\right) \sum_{I=1}^N \tilde{g}_{md}^{(I)} \left(\frac{2I}{3} + 1\right) \frac{2I}{3} \frac{2I-3}{3} \rho_0^{2I/3+1}. \quad (D3)$$

The fourth derivative of the energy per nucleon Z_0 is

$$Z_0 = 81\rho_0^4 \left. \frac{\partial^4 E/A}{\partial \rho^4} \right|_{\rho_0} = \frac{-168}{5}\epsilon_F^0 + 81\frac{\beta}{\gamma+1}\gamma(\gamma-1)(\gamma-2)(\gamma-3) + 81\left(\tilde{C}_0 + \frac{\tilde{D}_0}{2}\right) \sum_{I=1}^N \tilde{g}_{md}^{(I)} \left(\frac{2I}{3} + 1\right) \frac{2I}{3} \frac{2I-3}{3} \frac{2I-6}{3} \rho_0^{2I/3+1}. \quad (D4)$$

Around the normal nuclear density ρ_0 , the nuclear symmetry energy $S(\rho)$ can be similarly expanded (e.g., up to fourth order in x) as

$$S(\rho) = S(\rho_0) + Lx + \frac{K_{\text{sym}}}{2!}x^2 + \frac{Q_{\text{sym}}}{3!}x^3 + \frac{Z_{\text{sym}}}{4!}x^4 + O(x^5). \quad (D5)$$

The slope of the symmetry energy L is

$$L = 3\rho_0 \left. \frac{\partial S(\rho)}{\partial \rho} \right|_{\rho_0} = \frac{2}{3}\epsilon_F^0 + 3A_{\text{sym}} + 3B_{\text{sym}}\gamma + 3 \sum_{I=1}^N \tilde{C}_{\text{sym}}^{(I)} \left(\frac{2I}{3} + 1\right) \rho_0^{2I/3+1}. \quad (D6)$$

The curvature of the symmetry energy K_{sym} is

$$K_{\text{sym}} = 9\rho_0^2 \left. \frac{\partial^2 S(\rho)}{\partial \rho^2} \right|_{\rho_0} = -\frac{2}{3}\epsilon_F^0 + 9B_{\text{sym}}\gamma(\gamma-1) + 9 \sum_{I=1}^N \tilde{C}_{\text{sym}}^{(I)} \left(\frac{2I}{3} + 1\right) \frac{2I}{3} \rho_0^{2I/3+1}. \quad (D7)$$

The third derivative of the symmetry energy Q_{sym} is

$$Q_{\text{sym}} = 27\rho_0^3 \left. \frac{\partial^3 S(\rho)}{\partial \rho^3} \right|_{\rho_0} = \frac{8}{3}\epsilon_F^0 + 27B_{\text{sym}}\gamma(\gamma-1)(\gamma-2) + 27 \sum_{I=1}^N \tilde{C}_{\text{sym}}^{(I)} \left(\frac{2I}{3} + 1\right) \frac{2I}{3} \frac{2I-3}{3} \rho_0^{2I/3+1}. \quad (D8)$$

The fourth derivative of the symmetry energy Z_{sym} is

$$Z_{\text{sym}} = 81\rho_0^4 \left. \frac{\partial^4 S(\rho)}{\partial \rho^4} \right|_{\rho_0} = \frac{-56}{3}\epsilon_F^0 + 81B_{\text{sym}}\gamma(\gamma-1)(\gamma-2)(\gamma-3) + 81 \sum_{I=1}^N \tilde{C}_{\text{sym}}^{(I)} \left(\frac{2I}{3} + 1\right) \frac{2I}{3} \frac{2I-3}{3} \frac{2I-6}{3} \rho_0^{2I/3+1}. \quad (D9)$$

TABLE III. The parameters K_0 , Q_0 , Z_0 , K_{sym} , Q_{sym} , Z_{sym} are in MeV.

Parameter	(0.3, 46)	(−0.3, 46)	(0.3, 100)	(−0.3, 100)
K_0		230 (230)		
Q_0		−406.07 (−376.62)		
Z_0		1651.85 (1629.82)		
K_{sym}	−162.21 (−122.96)	−174.23 (−182.36)	41.72 (74.56)	29.70 (15.16)
Q_{sym}	363.94 (526.53)	422.23 (368.67)	−89.49 (63.90)	−31.20 (−93.97)
Z_{sym}	−2403.24(−3173.67)	−2203.28(−2033.33)	−34.78 (−702.16)	165.19(438.18)

In Table III, we list the values of these higher-order expansion coefficients of the nuclear matter equation that we used in this work. The values in brackets from the second to the seventh rows represent the values obtained with the standard Skyrme MDI.

- [1] A. W. Steiner, J. M. Lattimer, and E. F. Brown, The neutron star mass-radius relation and the equation of state of dense matter, *Astrophys. J. Lett.* **765**, L5 (2013).
- [2] J. M. Lattimer, The nuclear equation of state and neutron star masses, *Annu. Rev. Nucl. Part. Sci.* **62**, 485 (2012).
- [3] B. P. Abbott, R. Abbott, T. D. Abbott, F. Acernese, K. Ackley, and *et al.* (LIGO Scientific Collaboration and Virgo Collaboration), GW170817: Observation of gravitational waves from a binary neutron star inspiral, *Phys. Rev. Lett.* **119**, 161101 (2017).
- [4] L. Baiotti, Gravitational waves from neutron star mergers and their relation to the nuclear equation of state, *Prog. Part. Nucl. Phys.* **109**, 103714 (2019).
- [5] B. Margalit and B. D. Metzger, The multi-messenger matrix: The future of neutron star merger constraints on the nuclear equation of state, *Astrophys. J. Lett.* **880**, L15 (2019).
- [6] J. M. Lattimer and M. Prakash, The physics of neutron stars, *Science* **304**, 536 (2004).
- [7] H. Yasin, S. Schäfer, A. Arcones, and A. Schwenk, Equation of state effects in core-collapse supernovae, *Phys. Rev. Lett.* **124**, 092701 (2020).
- [8] A. W. Steiner, M. Hempel, and T. Fischer, Core-collapse supernova equations of state based on neutron star observations, *Astrophys. J.* **774**, 17 (2013).
- [9] K. Chatziioannou, Neutron-star tidal deformability and equation-of-state constraints, *Gen. Relativ. Gravitation* **52**, 109 (2020).
- [10] T. Malik, N. Alam, M. Fortin, C. Providência, B. K. Agrawal, T. K. Jha, B. Kumar, and S. K. Patra, GW170817: Constraining the nuclear matter equation of state from the neutron star tidal deformability, *Phys. Rev. C* **98**, 035804 (2018).
- [11] N. H. Tan, D. T. Khoa, and D. T. Loan, Equation of state of asymmetric nuclear matter and the tidal deformability of neutron star, *Eur. Phys. J. A* **57**, 153 (2021).
- [12] B.-A. Li, B.-J. Cai, W.-J. Xie, and N.-B. Zhang, Progress in constraining nuclear symmetry energy using neutron star observables since GW170817, *Universe* **7**, 182 (2021).
- [13] C. Y. Tsang, M. B. Tsang, W. Lynch, R. Kumar, and C. Horowitz, The nuclear equation of state from experiments and astrophysical observations, *Preprint (Version 1) available at Research Square*, (2023).
- [14] W.-J. Xie and B.-A. Li, Bayesian inference of high-density nuclear symmetry energy from radii of canonical neutron stars, *Astrophys. J.* **883**, 174 (2019).
- [15] Y. Zhang, M. Liu, C.-J. Xia, Z. Li, and S. K. Biswal, Constraints on the symmetry energy and its associated parameters from nuclei to neutron stars, *Phys. Rev. C* **101**, 034303 (2020).
- [16] J. W. Holt and Y. Lim, Dense matter equation of state and neutron star properties from nuclear theory and experiment, *AIP Conf. Proc.* **2127**, 020019 (2019).
- [17] H. Wolter *et al.* (TMEP Collaboration), Transport model comparison studies of intermediate-energy heavy-ion collisions, *Prog. Part. Nucl. Phys.* **125**, 103962 (2022).
- [18] A. Sorensen, K. Agarwal, K. W. Brown, Z. Chajecski, P. Danielewicz, C. Drischler, S. Gandolfi, J. W. Holt, M. Kaminski, C.-M. Ko, R. Kumar, B.-A. Li, W. G. Lynch, A. B. McIntosh, W. G. Newton, S. Pratt, O. Savchuk, M. Stefaniak, I. Tews, M. B. Tsang *et al.*, Dense nuclear matter equation of state from heavy-ion collisions, *Prog. Part. Nucl. Phys.*, **134**, 104080 (2024).
- [19] M. B. Tsang, Y. Zhang, P. Danielewicz, M. Famiano, Z. Li, W. G. Lynch, and A. W. Steiner, Constraints on the density dependence of the symmetry energy, *Phys. Rev. Lett.* **102**, 122701 (2009).
- [20] M. B. Tsang, J. R. Stone, F. Camera, P. Danielewicz, S. Gandolfi, K. Hebeler, C. J. Horowitz, J. Lee, W. G. Lynch, Z. Kohley, R. Lemmon, P. Möller, T. Murakami, S. Riordan, X. Roca-Maza, F. Sammarruca, A. W. Steiner, I. Vidaña, and S. J. Yennello, Constraints on the symmetry energy and neutron skins from experiments and theory, *Phys. Rev. C* **86**, 015803 (2012).
- [21] Y. Wang, Q. Li, Y. Leifels, and A. L. Fèvre, Study of the nuclear symmetry energy from the rapidity-dependent elliptic flow in heavy-ion collisions around 1 GeV/nucleon regime, *Phys. Lett. B* **802**, 135249 (2020).
- [22] M. D. Cozma, Feasibility of constraining the curvature parameter of the symmetry energy using elliptic flow data, *Eur. Phys. J. A* **54**, 40 (2018).
- [23] S. Huth, P. T. H. Pang, I. Tews, T. Dietrich, A. Le Fèvre, A. Schwenk, W. Trautmann, K. Agarwal, M. Bulla, M. W. Coughlin, and C. Van Den Broeck, Constraining neutron-star matter with microscopic and macroscopic collisions, *Nature (London)* **606**, 276 (2022).
- [24] Y. Liu, Y. Zhang, J. Yang, Y. Wang, Q. Li, and Z. Li, Impacts of momentum dependent interaction, symmetry energy and near-threshold $NN \rightarrow N\Delta$ cross sections on isospin sensitive flow and pion observables, *arXiv:2301.03066*.

- [25] B.-A. Li, C. B. Das, S. Das Gupta, and C. Gale, Effects of momentum-dependent symmetry potential on heavy-ion collisions induced by neutron-rich nuclei, *Nucl. Phys. A* **735**, 563 (2004).
- [26] J. Rizzo, M. Colonna, and M. Di Toro, Fast nucleon emission as a probe of the momentum dependence of the symmetry potential, *Phys. Rev. C* **72**, 064609 (2005).
- [27] Y. Zhang, M. Tsang, Z. Li, and H. Liu, Constraints on nucleon effective mass splitting with heavy ion collisions, *Phys. Lett. B* **732**, 186 (2014).
- [28] Z.-Q. Feng, Momentum dependence of the symmetry potential and its influence on nuclear reactions, *Phys. Rev. C* **84**, 024610 (2011).
- [29] J. Xu, L.-W. Chen, and B.-A. Li, Thermal properties of asymmetric nuclear matter with an improved isospin- and momentum-dependent interaction, *Phys. Rev. C* **91**, 014611 (2015).
- [30] B.-A. Li, C. B. Das, S. Das Gupta, and C. Gale, Momentum dependence of the symmetry potential and nuclear reactions induced by neutron-rich nuclei at RIA, *Phys. Rev. C* **69**, 011603(R) (2004).
- [31] A. M. Lane, Isobaric spin dependence of the optical potential and quasi-elastic (p, n) reactions, *Nucl. Phys.* **35**, 676 (1962).
- [32] Z. Zhang and C. M. Ko, Pion production in a transport model based on mean fields from chiral effective field theory, *Phys. Rev. C* **98**, 054614 (2018).
- [33] F.-Y. Wang, J.-P. Yang, X. Chen, Y. Cui, Y.-J. Wang, Z.-G. Xiao, Z.-X. Li, and Y.-X. Zhang, Probing nucleon effective mass splitting with light particle emission, *Nucl. Sci. Tech.* **34**, 94 (2023).
- [34] J. Aichelin, “Quantum” molecular dynamic—a dynamical microscopic n -body approach to investigate fragment formation and the nuclear equation of state in heavy ion collisions, *Phys. Rep.* **202**, 233 (1991).
- [35] J. Aichelin, A. Rosenhauer, G. Peilert, H. Stoecker, and W. Greiner, Importance of momentum-dependent interactions for the extraction of the nuclear equation of state from high-energy heavy-ion collisions, *Phys. Rev. Lett.* **58**, 1926 (1987).
- [36] Y. Zhang and Z. Li, Elliptic flow and system size dependence of transition energies at intermediate energies, *Phys. Rev. C* **74**, 014602 (2006).
- [37] Y. Wang, C. Guo, Q. Li, H. Zhang, Y. Leifels, and W. Trautmann, Constraining the high-density nuclear symmetry energy with the transverse-momentum-dependent elliptic flow, *Phys. Rev. C* **89**, 044603 (2014).
- [38] Y. Liu, Y. Wang, Y. Cui, C.-J. Xia, Z. Li, Y. Chen, Q. Li, and Y. Zhang, Insights into the pion production mechanism and the symmetry energy at high density, *Phys. Rev. C* **103**, 014616 (2021).
- [39] C. B. Das, S. Das Gupta, C. Gale, and B.-A. Li, Momentum dependence of symmetry potential in asymmetric nuclear matter for transport model calculations, *Phys. Rev. C* **67**, 034611 (2003).
- [40] M. D. Cozma, Y. Leifels, W. Trautmann, Q. Li, and P. Russotto, Toward a model-independent constraint of the high-density dependence of the symmetry energy, *Phys. Rev. C* **88**, 044912 (2013).
- [41] N. Ikeno and A. Ono, Collision integral with momentum-dependent potentials and its impact on pion production in heavy-ion collisions, *Phys. Rev. C* **108**, 044601 (2023).
- [42] M. Isse, A. Ohnishi, N. Otuka, P. K. Sahu, and Y. Nara, Mean-field effects on collective flow in high-energy heavy-ion collisions at 2–158A GeV energies, *Phys. Rev. C* **72**, 064908 (2005).
- [43] J. Su, L. Zhu, C.-Y. Huang, W.-J. Xie, and F.-S. Zhang, Correlation between symmetry energy and effective k -mass splitting with an improved isospin- and momentum-dependent interaction, *Phys. Rev. C* **94**, 034619 (2016).
- [44] L.-W. Chen, C. M. Ko, and B.-A. Li, Determination of the stiffness of the nuclear symmetry energy from isospin diffusion, *Phys. Rev. Lett.* **94**, 032701 (2005).
- [45] J. Rizzo, M. Colonna, V. Baran, M. Di Toro, H. Wolter, and M. Zielinska-Pfabe, Isospin dynamics in peripheral heavy ion collisions at Fermi energies, *Nucl. Phys. A* **806**, 79 (2008).
- [46] C. Hartnack and J. Aichelin, New parametrization of the optical potential, *Phys. Rev. C* **49**, 2801 (1994).
- [47] D. Davesne, J. Navarro, P. Becker, R. Jodon, J. Meyer, and A. Pastore, Extended Skyrme pseudopotential deduced from infinite nuclear matter properties, *Phys. Rev. C* **91**, 064303 (2015).
- [48] R. Wang, L.-W. Chen, and Y. Zhou, Extended Skyrme interactions for transport model simulations of heavy-ion collisions, *Phys. Rev. C* **98**, 054618 (2018).
- [49] Y. Zhang, N. Wang, Q.-F. Li, L. Ou, J.-L. Tian, M. Liu, K. Zhao, X.-Z. Wu, and Z.-X. Li, Progress of quantum molecular dynamics model and its applications in heavy ion collisions, *Front. Phys.* **15**, 54301 (2020).
- [50] Y. Zhang, Z. Li, and P. Danielewicz, In-medium NN cross sections determined from the nuclear stopping and collective flow in heavy-ion collisions at intermediate energies, *Phys. Rev. C* **75**, 034615 (2007).
- [51] S. Hama, B. C. Clark, E. D. Cooper, H. S. Sherif, and R. L. Mercer, Global Dirac optical potentials for elastic proton scattering from heavy nuclei, *Phys. Rev. C* **41**, 2737 (1990).
- [52] G. F. Bertsch, D. J. Dean, and W. Nazarewicz, Computing atomic nuclei: The universal nuclear energy density functional, *SciDAC Rev.* **6**, 42 (2007).
- [53] R. Furnstahl, The UNEDF project, *Nucl. Phys. News* **21**, 18 (2011).
- [54] B. G. Carlsson and J. Dobaczewski, Convergence of density-matrix expansions for nuclear interactions, *Phys. Rev. Lett.* **105**, 122501 (2010).
- [55] H. Mütter, R. Machleidt, and R. Brockmann, Dirac-Brueckner-Hartree-Fock approach in finite nuclei, *Phys. Lett. B* **202**, 483 (1988).
- [56] L. Ou, Z. Li, Y. Zhang, and M. Liu, Effect of the splitting of the neutron and proton effective masses on the nuclear symmetry energy at finite temperatures, *Phys. Lett. B* **697**, 246 (2011).
- [57] W.-C. Chen and J. Piekarewicz, Building relativistic mean field models for finite nuclei and neutron stars, *Phys. Rev. C* **90**, 044305 (2014).
- [58] P. Morfouace, C. Tsang, Y. Zhang, W. Lynch, M. Tsang, D. Coupland, M. Youngs, Z. Chajecki, M. Famiano, T. Ghosh, G. Jhang, J. Lee, H. Liu, A. Sanetullaev, R. Showalter, and J. Winkelbauer, Constraining the symmetry energy with heavy-ion collisions and Bayesian analyses, *Phys. Lett. B* **799**, 135045 (2019).
- [59] E. Chabanat, P. Bonche, P. Haensel, J. Meyer, and R. Schaeffer, A Skyrme parametrization from subnuclear to neutron star densities, *Nucl. Phys. A* **627**, 710 (1997).

- [60] Z. Zhang and L.-W. Chen, Isospin splitting of the nucleon effective mass from giant resonances in ^{208}Pb , *Phys. Rev. C* **93**, 034335 (2016).
- [61] Y. Nara, T. Maruyama, and H. Stoecker, Momentum-dependent potential and collective flows within the relativistic quantum molecular dynamics approach based on relativistic mean-field theory, *Phys. Rev. C* **102**, 024913 (2020).
- [62] J. Margueron, R. Hoffmann Casali, and F. Gulminelli, Equation of state for dense nucleonic matter from metamodelling. I. Foundational aspects, *Phys. Rev. C* **97**, 025805 (2018).
- [63] N. Glendenning, *Compact Stars: Nuclear Physics, Particle Physics and General Relativity*, *Astron. Astrophys. Library* (Springer, 1997).
- [64] D. D. S. Coupland, M. Youngs, Z. Chajecski, W. G. Lynch, M. B. Tsang, Y. X. Zhang, M. A. Famiano, T. K. Ghosh, B. Giacherio, M. A. Kilburn, J. Lee, H. Liu, F. Lu, P. Morfouace, P. Russotto, A. Sanetullaev, R. H. Showalter, G. Verde, and J. Winkelbauer, Probing effective nucleon masses with heavy-ion collisions, *Phys. Rev. C* **94**, 011601(R) (2016).
- [65] C. Xu, B.-A. Li, and L.-W. Chen, Symmetry energy, its density slope, and neutron-proton effective mass splitting at normal density extracted from global nucleon optical potentials, *Phys. Rev. C* **82**, 054607 (2010).
- [66] M. B. Tsang, W. A. Friedman, C. K. Gelbke, W. G. Lynch, G. Verde, and H. S. Xu, Isotopic scaling in nuclear reactions, *Phys. Rev. Lett.* **86**, 5023 (2001).
- [67] M. B. Tsang, C. K. Gelbke, X. D. Liu, W. G. Lynch, W. P. Tan, G. Verde, H. S. Xu, W. A. Friedman, R. Donangelo, S. R. Souza, C. B. Das, S. Das Gupta, and D. Zhabinsky, Isoscaling in statistical models, *Phys. Rev. C* **64**, 054615 (2001).
- [68] A. Ono, P. Danielewicz, W. A. Friedman, W. G. Lynch, and M. B. Tsang, Isospin fractionation and isoscaling in dynamical simulations of nuclear collisions, *Phys. Rev. C* **68**, 051601(R) (2003).
- [69] S. Das Gupta and A. Mekjian, The thermodynamic model for relativistic heavy ion collisions, *Phys. Rep.* **72**, 131 (1981).
- [70] G. Fai and A. Z. Mekjian, Minimal information and statistical descriptions of nuclear fragmentation, *Phys. Lett. B* **196**, 281 (1987).
- [71] A. S. Botvina, O. V. Lozhkin, and W. Trautmann, Isoscaling in light-ion induced reactions and its statistical interpretation, *Phys. Rev. C* **65**, 044610 (2002).
- [72] W.-H. Long, N. Van Giai, and J. Meng, Density-dependent relativistic Hartree-Fock approach, *Phys. Lett. B* **640**, 150 (2006).
- [73] M. Colonna, Y.-X. Zhang, Y.-J. Wang, D. Cozma, P. Danielewicz, C. M. Ko, A. Ono, M. B. Tsang, R. Wang, H. Wolter, J. Xu, Z. Zhang, L.-W. Chen, H.-G. Cheng, H. Elfner, Z.-Q. Feng, M. Kim, Y. Kim, S. Jeon, C.-H. Lee *et al.*, Comparison of heavy-ion transport simulations: Mean-field dynamics in a box, *Phys. Rev. C* **104**, 024603 (2021).
- [74] Y.-X. Zhang, Y.-J. Wang, M. Colonna, P. Danielewicz, A. Ono, M. B. Tsang, H. Wolter, J. Xu, L.-W. Chen, D. Cozma, Z.-Q. Feng, S. Das Gupta, N. Ikeno, C.-M. Ko, B.-A. Li, Q.-F. Li, Z.-X. Li, S. Mallik, Y. Nara, T. Ogawa *et al.*, Comparison of heavy-ion transport simulations: Collision integral in a box, *Phys. Rev. C* **97**, 034625 (2018).
- [75] A. Ono, J. Xu, M. Colonna, P. Danielewicz, C. M. Ko, M. B. Tsang, Y.-J. Wang, H. Wolter, Y.-X. Zhang, L.-W. Chen, D. Cozma, H. Elfner, Z.-Q. Feng, N. Ikeno, B.-A. Li, S. Mallik, Y. Nara, T. Ogawa, A. Ohnishi, D. Oliinychenko *et al.*, Comparison of heavy-ion transport simulations: Collision integral with pions and Δ resonances in a box, *Phys. Rev. C* **100**, 044617 (2019).
- [76] Y. Zhang, D. D. S. Coupland, P. Danielewicz, Z. Li, H. Liu, F. Lu, W. G. Lynch, and M. B. Tsang, Influence of in-medium nn cross sections, symmetry potential, and impact parameter on isospin observables, *Phys. Rev. C* **85**, 024602 (2012).
- [77] C. Aidala, A. Aprahamian, S. Bacca, P. Bedaque, L. Bernstein, J. Carlson, M. Carpenter, K. Chippis, V. Cirigliano, I. Cloët, A. de Gouvea, R. deSouza, G. Dodge, E. J. Downie, J. Dudek, R. Fatemi, A. Gade, H. Gao, S. Gardner, S. V. Greene *et al.*, *A New Era of Discovery: The 2023 Long Range Plan for Nuclear Science (V.1.3)* (Nuclear Science Advisory Committee, Washington, DC, USA, 2023).